AD-A244 466

IENTATION PAGE

Form Approved
OMB No 0704-0188

itimated to average 1 hour per response, including the time for reviewing instructions, searching existing data sources, ind reviewing the collection of information. Send comments regarding this burden estimate or any other aspect of this this burden to Washington Headquarters Services, Directorate for Information Operations and Reports, 1215 Jefferson the Office of Management and Budget, Paperwork Reduction Project (0704-0188), Washington, DC 20503

1. AGENCY USE ONLY (Leave blank)	2. REPORT DATE	3. REPORT TYPE AND DATES COVERED
	31 October 91	FINAL, 9-1-89 to 9-30-91

4. TITLE AND SUBTITLE
Investigating Digital Optical Computing with Spatial Light Rebroadcasters

5. FUNDING NUMBERS
AFOSR-89-0525

DTIC
ELECTE
JAN 16 1992
S D
D

6. AUTHOR(S)
Alastair D. McAulay (PI)
Junqing Wang, Xin Xu

7. PERFORMING ORGANIZATION NAME(S) AND ADDRESS(ES)
Professor Alastair D. McAulay
Wright State University
Department of Computer Science and Engineering
Dayton, OH 45435

8. PERFORMING ORGANIZATION REPORT NUMBER
WSU-CS-91-11

AFOSR 91 1026

9. SPONSORING/MONITORING AGENCY NAME(S) AND ADDRESS(ES)
Dr. Alan E. Craig
AFOSR/NE
Building 410
Bolling AFB, Washington, DC 20332-6448

10. SPONSORING/MONITORING AGENCY REPORT NUMBER
2305/B1

11. SUPPLEMENTARY NOTES

This document has been approved for public release and sale; its distribution is unlimited.

12a. DISTRIBUTION/AVAILABILITY STATEMENT

unlimited

92-01023

13. ABSTRACT *(Maximum 200 words)*

Spatial light rebroadcasters (SLRs), consisting of thin films of luminescing electron trapping materials, are ecxlored for digital optical computing. The status of optical computing is reviewed briefly. SLRs are characterized in detail; fabrication, sensitivity, linearity, speed, resolution, and modulation. A number of optical experiments are described that were conducted to determine the device effectiveness, applications for which the devices are best suited, and the direction for research to develop more useful devices. Optical experiments with basic SLR modules include a cascadable module, binary matrix-vector multiplier, and correlator. The basic modules were then used in memory, adder, interconnection, and learning experiments. These experiments show that the SLR has potential for digital optical computing, particularly where high density long term storage is required. However, the lack of gain, incoherent output, and lot output signals, means that other collaborative devices are needed which limit the performance. Future directions are discussed.

14. SUBJECT TERMS	15. NUMBER OF PAGES
Optical Computing, Spatial Light Rebroadcaster, Optical Memory, Associate Memory, Luminescence.	56
	16. PRICE CODE

17. SECURITY CLASSIFICATION OF REPORT	18. SECURITY CLASSIFICATION OF THIS PAGE	19. SECURITY CLASSIFICATION OF ABSTRACT	20. LIMITATION OF ABSTRACT
UNCLASSIFIED	UNCLASSIFIED	UNCLASSIFIED	UL

Contents

Accesion For
NTIS CRA&I
DTIC TAB
Unannounced
Justification
By
Distribution /
Dist

Foreword

The work reported was performed by Wright State University Computer Science and Engineering Department under contract AFOSR-89-0525 with the Air Force Office of Scientific Research. Dr. Alan E. Craig was the Air Force project manager and Dr. Alastair D. McAulay, NCR Distinguished Professor and Chairman of the Department of Computer Science & Engineering was the Principal Investigator. Technical contributors from Wright State also included Mr Junqing Wang, and PhD students Xin Xu, and M. Zeng. In addition, Dr George Storti of Quantex provided consultation and contributed to the information on the spatial light rebroadcaster material.

1 Introduction

Scientific and non-scientific computer users continue to desire faster computers with increased memory and faster communication links to other computers. Digital computers require memory, interconnection and logic, as well as control and programming strategies. Computer engineers are increasingly adopting optical fibers for interconnections because of higher bandwidths and communication speeds, both for interconnecting processors and for local area networks. Optical disk is likely to replace magnetic disk for memory because of ease of access to the disk. Optic and electrooptic integrated optics are in development that incorporate microlasers [32] and GaAs devices [57],[72]. Microlasers provide a mechanism for communicating higher bandwidth signals out of VLSI chips with less power than is required with conventional electronic pins. This becomes increasingly important as the density of active elements on a chip increases. These advances in a wide range of optical technologies suggest that optical digital computers will compete favorably with all electronic digital computers in the future. In this report, optical digital computers refers to digital computers with significant optical involvement. At this time, there are many devices and strategies and it s unclear which combination of devices and approaches will eventually prove supe .or [48].

In this report, we investigate the use of new high speed, high resolution devices, referred to as spatial light rebroadcasters (SLRs), having a thin film of electron trapping material. SLRs have the potential for low cost, nanosecond speeds, and micron resolution. Further, they allow 2-D optical addressing, and indefinite storage. The characteristics of the material and its use in digital optical computing has not been investigated in detail elsewhere to our knowledge. No other 2-D optically addressable devices appear to have this kind of resolution and speed. However, these devices are difficult to use because of their attenuation and lack of gain, low output signals, incoherent output, and use of multiple wavelength sources. We investigate the effectiveness of the devices for digital optical computing, the applications for which the devices are best suited, and the direction for research to develop more useful devices.

Section 2 provides a brief status review of optical digital computing and background on the use of optics for memory, address, interconnections, and learning. SLR fabrication and measurements of sensitivity, linearity, speed, and modulation, are described in section 3. In section 4, optical experiments are reported for three basic SLR modules: cascadable module, binary matrix-vector multiplier, and binary correlator. These basic modules are used in section 5 for optical experiments on memory, adders, interconnections, and learning. Future research and conclusions are presented in sections 6 and 7 respectively.

2 Background

We discuss briefly the use of optics for digital computing, memory, interconnections, arithmetic, and learning. The use of spatial light rebroadcasters is discussed.

2.1 Status of optical digital computing

The transition to all optical digital computers, in which optics is dominant, will be difficult because of the infrastructure and momentum of existing electronic computers and associated software. Optical enhancements to solve specific problems in electronic computers are more likely to occur first. Examples include: on chip optical communication, optical clock distribution, and optical connections on and off chips to overcome pin limitations. Optical learning to alleviate the software crisis will require a more significant optical component. Optics may be appropriate for learning because the requirements on dynamic range and uniformity are less.

Alternative approaches include the use of free space, microoptics, integrated optics, and fibers. In this report we use free space which effectively utilizes a third dimension in moving data between 2-D arrays. For robustness, free space may be replaced by bulk transparent materials including glass and photorefractive crystals. The system is then reduced to microoptic in order to increase speed. Light takes a nanosecond to travel a foot in space or a few inches in materials with higher refractive index. Microoptics research involves the development of new materials and effective fabrication techniques for miniature optical designs [28],[32]. In some structures, 2-D GaAs VLSI chips have detectors and microlasers on both sides for interfacing with other chips. The chips are placed one on top of the other, using etched alignment pins, or optical alignment detectors and transmitters, so that 2-D information flows through them in sequence. A feedback loop allows extended computations. The use of modules is also critical for constructing cost effective systems. Research in microoptics is currently a significant activity at MIT Lincoln Laboratories, A.T. & T, Bellcore, Erlangen University [5], Nippon, Corning [4], and Matsushita [70]. Free space interconnections appear to have potential for multichip modules in which many chips are placed in a single package to reduce packaging costs and improve interconnection performance [7].

A second approach, considered by some as part of microoptics, involves optical integrated circuits (OICs). Optoelectronic integrated circuits (OEICs) include electronic and optical devices on the same chip. A.T. & T has an integrated optic repeater for fiber communications. Photonic integrated optics (PICs) have optical devices that communicate along optical waveguides [38] and minimal emphasis on electronics in the chip. Optical integrated circuits have the advantage of using techniques from integrated electronics. Circuits in an OIC are constrained to planar arrangements

or a few layers, which is a disadvantage unless parallel optical interfaces are used. For example, 2-D integrated optic devices may be concatenated by stacking as in a microoptic architecture described previously.

A third approach involves the use of optical fibers. Advantages relative to other approaches include the avoidance of diffraction losses and the ability to move data from any point to any other. Further, because energy is trapped in the fiber, it is possible to make use of chromatic dispersion, modal birefringence, or other nonlinear effects. The latter include self phase and cross phase modulation due to variations of refractive index with intensity, and stimulated Raman and Brillouin scattering [2]. The unstable equilibrium between anomalous dispersion and nonlinearity, required to generate solitons, is reminiscent of other self organizing systems studied in neural networks. An interesting effect for optical digital computing is that we can perform logic while moving data [29]. In contrast, current computers require several steps; fetch data, temporarily store data, perform computations and then store data for later use. A disadvantage of fibers is the increased cost and decreased reliability associated with large numbers of connectors.

An alternative approach to optical enhancement is specialized optical processors. This is appropriate for high speed and where large amounts of data are processed with seldom changing algorithms, such as in digital signal processing. This makes precompiling and optimization of architecture possible [48](Chapter 14). Examples of special purpose systems include integrated optic acousto-optic spectrum analyzers [25], phased-array antenna signal processors [65], and novel sonar processors [49].

Progress in optical computing is dependent on collaboration between experts in a wide range of technologies, including computer scientists, computer engineers, and the optical computing community [48]. The next section discuss background on optical memory, adders, interconnections and learning.

2.2 Background for optical subsystems

2.2.1 Optical memory

Desirable features for memory are: low cost, low energy, high density, and high speed. Further, desired information must be readily accessible. Optics has demonstrated its superiority for access in disk technologies, where focusing of light through the disk surface avoids the physical closeness required in magnetic disk. The potential for optics is in parallel access.

A major difficulty with parallel electronic computers based on a shared memory paradigm is contention during parallel access for read and write. In a parallel random access memory (PRAM) model, if two processors request data from the same memory cell, it must be determined who asked first. The second request must then be queued

and serviced later. This adds considerable complexity and cost to memory access. It can be shown that certain algorithms can be made significantly faster if parallel write and read is available. An example is the algorithm for finding the root for the nodes in a tree, which is $O(log_2(width)/log_2(depth))$ faster if parallel reads are available [8], as in a concurrent read PRAM (CRPRAM). The finding of the maximum of n numbers using n^2 processors is no faster with concurrent reads, but can be faster by $O(log_2 n)$ if parallel reads are available in a concurrent write PRAM (CWPRAM). A major advantage of optics is the potential to write and read into the same memory location simultaneously from several processors [48](Chapter 13). A pattern on a piece of film can be imaged to different detectors associated with different processors, because there is no interference between light paths passing through the film at different angles.

Parallel access permits fast, cost effective associative memory for replacing slower random access memory. Associative memory is used in electronic computing where high speed is considered worth the extra cost, such as in cache and virtual memory translation look-aside-buffers [48]. The space-time bandwidth is not expected to be sufficient using optical devices alone. Therefore, mechanical motion aids are anticipated in memory design.

Associative memory [36] has been investigated by many researchers, for example, holographic [15], symbolic substitution [5][24], template matching [30][54], bidirectional [37] and matrix-vector [3][73][6]. Photorefractive crystals are being used for holographic storage experiments [23]. Learning with photorefractive crystals was demonstrated in reference [64] and [62]. Autoassociative memories have been demonstrated in reference [64][62]. In this report, we illustrate orthogonal memory [51]and bit-slice searching [53].

2.2.2 Optical adders

Adders are basic arithmetic units from which other arithmetic operations are derived [48](Chapter 10). Floating point computations involve complex operations that can be performed more cost effectively in electronics at this time, so that hybrid optical-electronic systems are attractive [48](Chapter 14). We concentrate on optical fixed point adders. In order to construct adders we need to be able to perform logic. All 16 possible logic operations between two operands have been demonstrated with SLRs [51]. A half adder was demonstrated with SLRs [46],[47].

An optical half adder computes the sum s_i and the carry c_i:

$$\begin{aligned} s_i &= a_i \oplus b_i \\ c_i &= a_i \cdot b_i \end{aligned} \tag{1}$$

where $\oplus$ is the exclusive OR (XOR) operation. Upper case bold face letters will be used to indicate 2-D arrays, each element of which performs the operation of equation (1).

Liquid crystal devices have been used to perform a parallel half adder [44]. In this case, the carry, $\mathbf{A} \cdot \mathbf{B}$ is computed first. The sum $\mathbf{A} \oplus \mathbf{B}$ is computed from $\mathbf{A} \cdot \overline{\mathbf{B}} + \overline{\mathbf{A}} \cdot \mathbf{B}$. In another half adder [13], two liquid crystal devices are used in series. If a pixel position is not set on both devices, there is no polarization change, so light passes through a matching analyzer. If a pixel position on either device is set, the polarization will change by 90^0 and no light will pass. If a pixel position on both devices is set, there will be a polarization change of 180^0 so that light will again pass through the analyzer. The inverse of the *carry* is computed by an OR operation between the *sum* and the inverse of one of the inputs, as can be seen by an examination of the truth tables. Parallel half adders have been proposed that use programmable logic array concepts, fan in and out limited to two, and SEEDs [58],[48](Chapter 10).

Half adders may be used to create full adders. The sum for a full adder is computed from:

$$s = a \oplus b \oplus c \tag{2}$$

where $\oplus$ means *exclusive OR* (XOR). The carry may be computed from:

$$c' = a \cdot b + a \cdot c + b \cdot c \tag{3}$$

A ripple-carry full adder causes the carry to ripple from the least significant bit to the most significant bit as the iterations proceed. This can be accomplished by adding a feedback path from the output of a half adder to its input [27]. A parallel ripple carry adder, using a programmable logic array concept and fans limited to two, was proposed in reference [71]. A ripple-carry full adder system using pattern logic was introduced in reference [74]. The power of pattern logic is that an attribute plane is used to specify different operations on a plane of data. As a result, the optics performs only shift invariant operations instead of shift variant ones. Symbolic substitution [5] has been used for a ripple carry adder. A video camera and computer for feedback were used with SLRs [34].

2.2.3 Optical interconnections

Optical interconnections may be used at all levels of computing. In many VLSI chips, 70% of the silicon area is devoted to interconnections and related tasks. By introducing free-space for connecting components on a chip, the third dimension is used in place of chip area [17],[12],[42]. In this case, electronic pathways are replaced by light traveling through free-space using LEDs, microlasers, detectors, and holograms. The optical path dissipates less energy than an electronic path when microlaser sources are used. Alternatively, optical waveguides may be used on a chip in place of a wire. This is not beneficial for lengths under 2 mm [11].

Optics has been proposed for connecting chips in multi-chip modules or individually packaged chips or other components on a board [26], [39],[63]. Clock skew can be

reduced by making all optical links the same length. Components on a board may be connected optically by using the third dimension [7],[19],[56]. Selfoc lenses are used to construct and optical bus for connecting circuit boards [20]. Boards are mounted so that detectors and emitters at one edge fit into slots in the optical bus.

2.2.4 Optical learning

Optics looks promising for neural network applications because of the potential massive parallelism and the ability to provide high speed interconnections. Optical architectures for implementing already trained neural networks are relatively simple and matrix-vector multipliers, correlators or associative memories may be used. As learning is computationally demanding, the higher performance of an optical computer would be useful [48](Chapter 16,17,18). We consider supervised learning in which a teacher is used to correct the weights during training.

The Perceptron algorithm learns to classify linearly separable classes of objects with a single layer. Optical experiments with photorefractive materials have been demonstrated [64]. We adopt this algorithm for use with spatial light rebroadcasters (SLRs) in section 5. SLRs are suitable because weights can be individually increased in parallel by writing and decreased in parallel by reading.

Backpropagation allows learning to classify objects that are not linearly separable by using multiple layers and backpropagating the error signals. An optical implementation is discussed in reference [64].

Feedforward neural networks act as associative memories and are trained to associate input and output patterns. We consider an orthogonal memory in section 5 in which orthogonal input patterns are associated with different output patterns. This is a heteroassociative memory. The weights are computed by an optical outer product and recall is by matrix-vector multiplication. A self or autoassociative memory provides an output when an imperfect or incomplete input is provided. If the input is in vector form, we first premultiply by a matrix $\mathbf{M}^T$ that has templates for different classes as its rows. The resulting correlation coefficients indicates how much of each template is present in the input. This can be used to classify by selecting the maximum correlation coefficient. These coefficients are now premultiplied by the matrix $\mathbf{M}$. Nonlinear feedback now reduces the smaller signals associated with the weaker correlations. After a number of iterations the template closest to the original input will dominate at the output. This was implemented in the space domain [43], using holograms with phase conjugate mirrors [62], and using angle holograms [1]

The premultiplication by $\mathbf{M}^T$ followed by premultiplication by $\mathbf{M}$ can be collapsed to premultiplication by the outer product matrix $\mathbf{M}\mathbf{M}^T$. In this case the network reduces to a Hopfield network. This network was modified for unipolar numbers and implemented optically in reference [10].

2.3 Advantages and disadvantages of SLRs

We should not expect a single SLR to have all desirable features such as high resolution, high switching speed, low switching energy, long term and short term storage capability, high contrast or dynamic range, low energy loss, and low cost. In order to be cost effective, conventional computers use a variety of diverse technologies, including for example, magnetic disk, semiconductor memory, and display technologies. A key to designing competitive digital optical computers involves skill in merging several optical and electronic devices in such as a way as to utilize their best features and be relatively independent of their poorer characteristics, while providing a high overall performance.

In this report we concentrate on the potential role of spatial light rebroadcasters in digital optical computing. SLRs are relatively inexpensive and have high resolution and speed. Experiments require sources of several wavelengths and the ability to handle low power light signals. These skills are expected to be useful for investigating other devices.

SLRs appear to be best suited to memory because there may be as many as 10^5 trapping sites in a cubic micron of electron trapping material. The rapid recovery of information from memory is important. This requires logic computation in the form of decoding addresses or matching. Performing the logic locally in the memory is more efficient because it avoids moving large amounts of unneeded data. Therefore, memory involves: integration with logic for matching, and interconnections to move data at high speed. SLRs appear to have the highest combination of resolution and speed of any device currently available. Later we show manipulation of 10,000 pixels in parallel on a one inch square SLR.

Major disadvantages of SLRs are the inefficiency in reading and the lack of gain. The luminescing energy on reading is limited by the number of electrons trapped during writing. As any optical system incurs loss, it is necessary to include a gain device when reading an SLR. The gain device does not require memory but should have equal resolution and comparable speed if the system is to achieve high performance.

A further disadvantage of SLRs is that they emit incoherent light when activated during reading. Therefore, the energy is emitted in a wide beam pattern following a square spreading law based on $4\pi r^2$, the area of a sphere of radius r. Large aperture lenses, or fiber optic plates, are needed to minimize energy loss. These capture more of the emitted light for subsequent processing. Later we show how a module may be constructed that provides memory, gain, interconnection and coherent input/output. Experimental results show memory, arithmetic, and interconnections possible using this module

3 Characteristics of spatial light rebroadcasters

Spatial light rebroadcasters (SLRs) consist of a thin film of electron trapping material (ET). These materials are also known as luminescent, or optically stimulable phosphors. We describe the fabrication and operation of these devices. Results are presented for measurements of sensitivity, linearity, speed, and resolution. We explain how these devices can be used to perform logic.

3.1 Fabrication and operation

We first explain the nature and fabrication of electron trapping materials and then how they function.

3.1.1 Fabrication

The particular ET material in our experiments is Calcium Sulfide (CaS) or Strontium Sulfide (SrS) which is doped with europium (Eu) and samarium (Sm). SrS is an indirect bandgap semiconductor with a bandgap of 4.3eV. Europium and samarium introduce energy levels in the forbidden gap of the SrS. At thermal equilibrium, the europium is in its 2+ valence state and samarium in its 3+ state. Blue light exposure excites an electron transition from the ground state of the Eu^{2+} to an excited state. If there are SM^{3+} atoms sufficiently close to the Eu^{2+} atoms, a tunneling transition occurs which eventually results in the electrons residing in samarium ground state energy levels. This means that Eu^{2+} has converted to Eu^{3+} and Sm^{3+} to Sm^{2+} as a consequence of the charge exchange. The transferred electron can remain at the samarium for very long times because the energy level is deep and transitions to the valence band are apparently forbidden. Near infrared light (NIR) exposure, however, is capable of exciting the electrons trapped at the samarium to an excited state of the samarium from whence the electrons transfer back to the excited states of the europium. In a very short time, the electrons fall to the lowest energy level of the Eu^{2+} excited states and then make a transition back to the ground state of the Eu^{2+} accompanied by the emission of orange light. With this NIR light exposure, the material returns to the state existing prior to blue light exposure - in other words, $Eu^{3+} \rightarrow Eu^{2+}$ and $Sm^{2+} \rightarrow Sm^{3+}$. Given the nature of the processes involved, complete reversibility exists - that is, it is possible to cycle the material indefinitely. Transition times will be fast since either tunneling processes or highly allowed electric dipole transitions are involved. We have measured the response time to the NIR light stimulation to be as short as 20 - 30ns.

The spectral sensitivities and emission of SrS:Eu,Sm are seen in Figure 1. The most efficient wavelength for generating the trapped electrons at samarium sites is

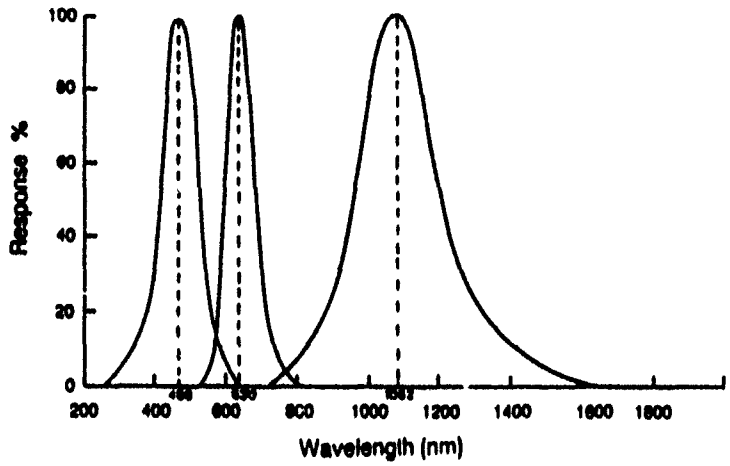

Figure 1: Spectral dependence of the emission, visible, and IR sensitivity of SrS:Eu, Sm

450nm: the most efficient wavelength for producing the orange emission is 100nm.

Since tunneling transitions will take place over only a few lattice constants, the ultimate achievable resolution will be limited by other factors such as the wavelengths of light employed, the thickness of the ET thin film, system configuration, etc. Consequently, images with micrometer size resolution are capable of being captured and read-out.

Another implication of the extremely small dimensions over which the electronic processes take place, along with the density of the dopants, is that a large dynamic range is expected for even micron sized pixels. From transmission and reflection measurements along with measurement of dopant concentrations, we have calculated that approximately 10^5 trapping centers exist per cubic micrometer. The specific processes taking place have been found to result in a linear dependence of the emission on both the blue and NIR light inputs, as discussed later. Consequently, it is possible to record an analog image with a dynamic range of many orders of magnitude as well as digital images with very high contrast.

As discussed later, approximately 10 mJ/cm^2 of 488nm light is required to saturate the electron traps in the ET thin film. More recent measurements have indicated that saturation is reached after an exposure of 4 mJ/cm^2. A further reduction in energy density required for saturation would result if the input wavelength were closer to 450nm. Approximately 10 times this energy is needed to deplete the electron traps to one percent of the saturated value (50-100 mJ/cm^2 of NIR light centered around 1000nm.)

An ET-SLM is easily fabricated. For example, powders of SrS, the chlorides of Eu and Sm, and LiF are obtained from vendors, and are thoroughly mixed in a ball mill for several hours. The resulting very fine powder is placed into a graphite crucible

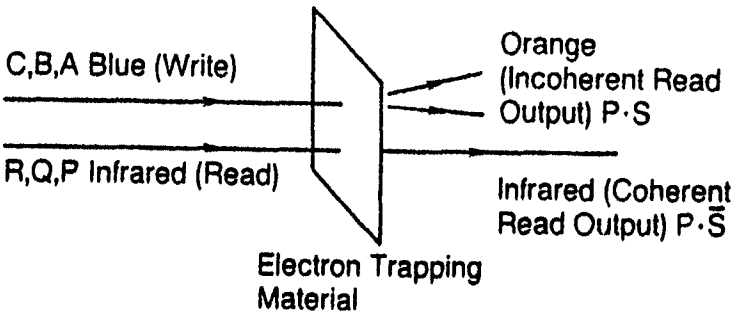

Figure 2: Operation of spatial light rebroadcaster

which in turn is placed into a programmable furnace. The temperature is raised above 850°C for an hour and then subsequently reduced to room temperature. Nitrogen gas provides the furnace ambient atmosphere. As a result of this process, the powders consolidate into a dense crystalline ingot with uniform properties.

A piece of an ingot is then placed into the hearth crucible of an electron beam deposition system. Substrates ($BaFl_2$, glass, or sapphire) are placed in a holder approximately 30cm from the source material. The films are deposited at a rate of 1.5 to 2.0 nm/s onto heated substrates. After the appropriate thickness is reached, the devices are allowed to cool to near room temperature before removal from the system.

Over the duration of the AFOSR contract, Quantex has made extensive investigations of those factors that impact critical performance parameters - i.e., the upconversion efficiency, the resolution, the retention of trapped electrons and energy input requirements. The factors that have been found to be important include the doping and flux concentrations, the temperature and the time at a particular temperature for producing the crystalline ingot, the electron beam deposition rate, and the substrate temperature.

3.1.2 Operation

The samples used in this report consist of a layer of alkali earth sulfide, such as CaS or SrS, containing selected dopants and deposited on a sapphire or $BaFl_2$ substrate. The operation is illustrated in figure 2. Electrons are trapped at those points in the material that are exposed to light of a given wavelength. The number of electrons trapped is proportional to the light intensity over a wide range of intensities. On exposing to a second wavelength, incoherent luminescence at a third wavelength occurs at those points where electrons were trapped. Further, for thin samples, analysis shows that the luminescence at each point is proportional to the product of the number of electrons trapped and the intensity of the second wavelength. This enables the material to perform multiplication on arrays. Samples used included a 250 μm thick

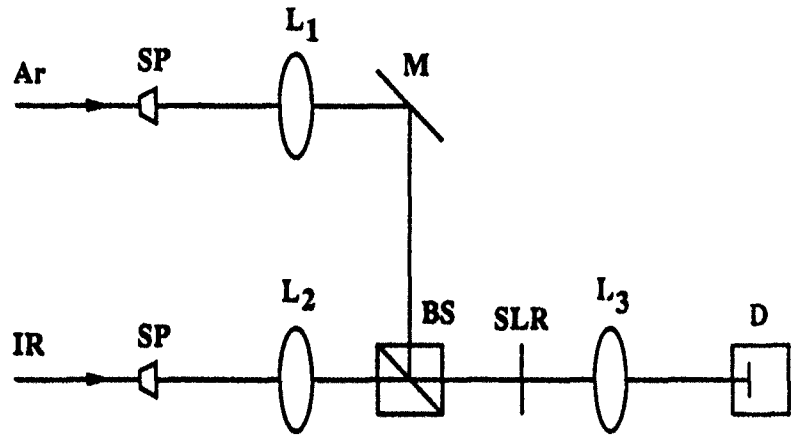

Figure 3: Optical set up for sensitivity experiments

CaS film, a 6 μm thin CaS film, and a thin SrS film. Basic properties and the ability to perform logic, addition, and multiplication with SLRs are described next.

3.2 Basic Properties

Basic properties include material sensitivity, linearity, resolution, reading, and writing speed, and modulation.

3.2.1 Material sensitivity and linearity

The optical set up for measuring sensitivity of the material is shown in figure 3. An orange bandpass filter is used at the output. During writing with thin fiml, the output intensity, consisting of orange luminescence and transmitted blue light is approximately 0.02% of the incident light from the argon laser. This does not present a problem because it occurs only during writing. Approximately 0.035% of the infrared light passes through the material and orange bandpass filter. This is larger than the intensity from the luminescence and has to be subtracted from the measurements.

The write and read intensity were measured in front of the material labeled SLR. The write energy was varied by controlling the exposure time from the argon laser using fixed intensity. On reading with IR, the orange luminescence and the IR pass through the SLR and are imaged without scaling onto the power meter D. The power meter is read immediately after the IR is switched on and again after the IR has been on sufficiently long to remove most of the trapped electrons. The two readings are subtracted to obtain a measurement for orange luminescence.

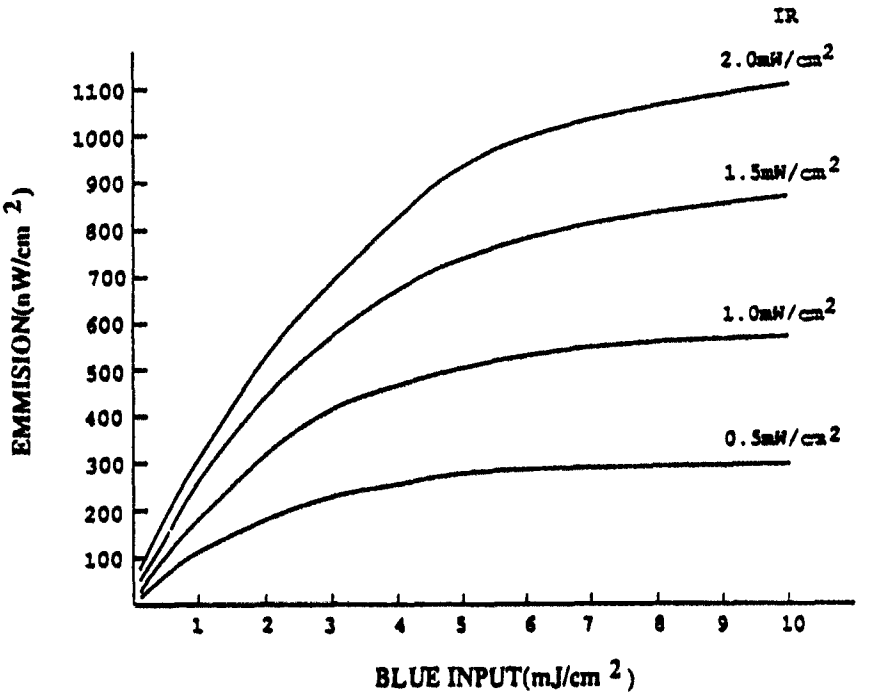

Figure 4: Output luminescence for thick CaS film

The results presented here are more detailed than those presented previously [51]. The output intensity for the orange luminescence, as a function of the blue write energy, is shown in figure 4 and figure 5 for thick and thin CaS films respectively. Different fixed IR read intensities are used for each case. The thick film can store more electrons and therefore a higher write energy is needed to reach saturation. Consequently, higher output luminescence may be achieved by illuminating with brighter IR during read.

The SrS sample has a higher transparency for IR than the CaS samples. In this case it is harder to separate the IR from the orange when measuring the orange luminescence behind the sample. Therefore, we used the set-up shown in figure 6 in which the detector is placed in front of the SLR sample. The resulting luminescence as a function of write energy is shown in figure 7.

The output intensity is more linear with input write energy for the thin film CaS, figure 5, and thin film SrS, figure 7, than for the thick film CaS, figure 4. We have measured a range of 100 to 1 for the linear portion. Using lower write intensities will increase the range of linearity. The linearity makes it possible to add numbers by writing on the material with intensities proportional to the numbers. The output will be approximately the sum of that for each number separately.

The output also varies linearly with IR read intensity for the thin film as can be seen, for example in figure 7, by examination of the variation of output for 0.5 mJ/cm^2 write energy and 1 to 2 mW/cm^2 IR read power. This permits multiplication

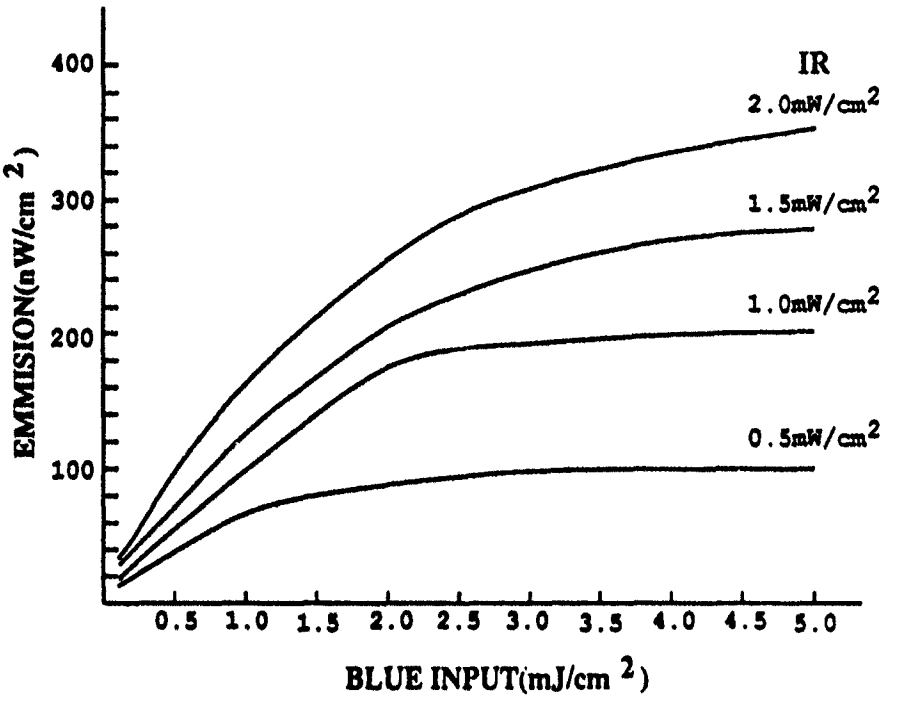

Figure 5: Output luminescence for thin CaS film

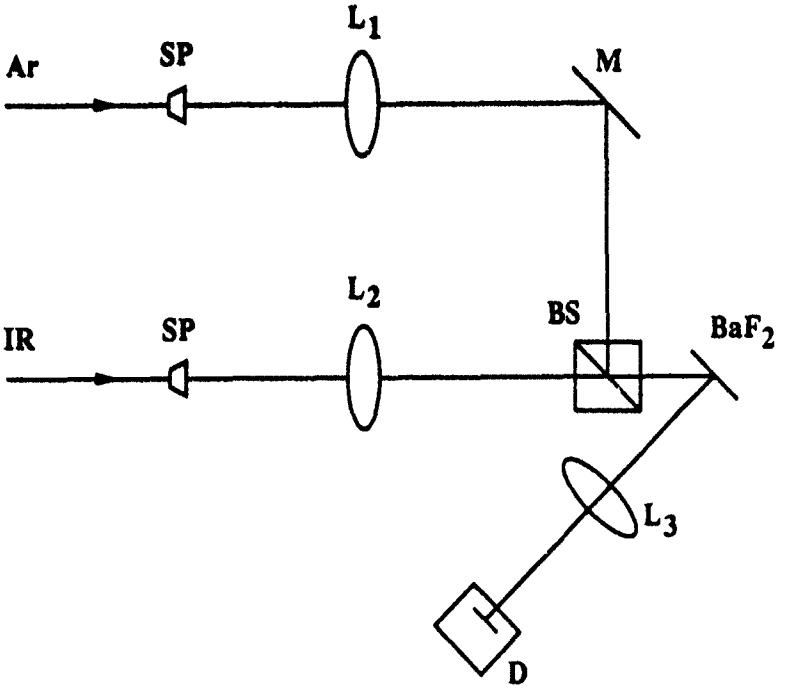

Figure 6: Optical set-up for measuring luminescence of SrS

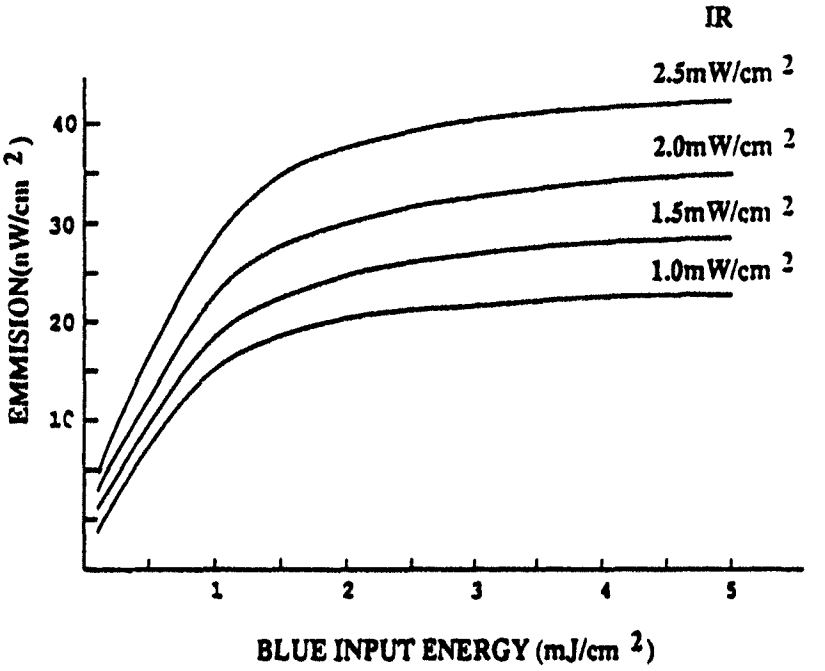

Figure 7: Output luminescence for thin SrS film

because the output y increases in proportion to write intensity w and read intensity r:

$$y = kwr \tag{4}$$

where k is a constant.

3.2.2 Writing speed, reading speed, and resolution

The optical set up for measuring writing speed is shown in figure 8. An acoustooptic cell was used to provide a 100 ns gate pulse for controlling the beam from an Argon laser. A photomultiplier tube was used for measurement. The upper oscilloscope trace in figure 9 shows the 100 ns write pulse. The lower trace shows that the orange luminescence responds in less than 100 ns. For this experiment, the infrared illumination was continuous. Therefore, any orange luminescence due to writing overlaps that due to reading.

Experiments with resolution charts, reported previously [51], show resolution for the thin film of 11 line-pairs/mm, comparable with a laser printer. A further experiment was performed using an x-y scanning mirror system controlled by an IBM/PS2 computer. Figure 10 shows the optical set-up: The write light from an argon laser is focussed by lens L_1 onto an acoustooptic cell, A-O, and then collimated by lens L_2. The x-axis mirror of the scanning mirror, SM, is controlled by the computer to move in a continuous manner. The y-axis mirror is moved in discrete steps to provide a

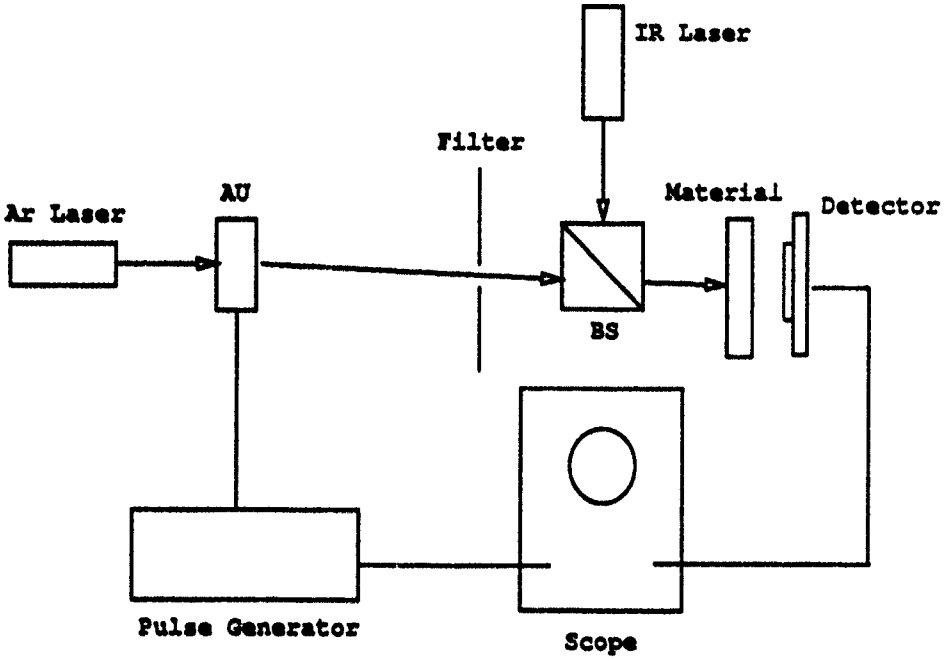

Figure 8: Optical set up for testing writing speed

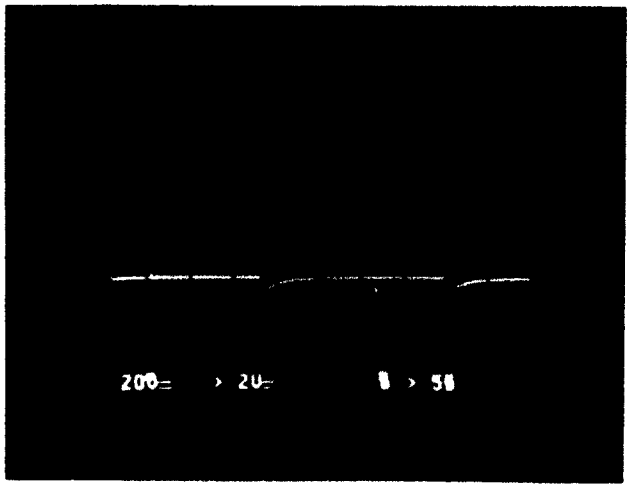

Figure 9: Oscilloscope result showing write speed

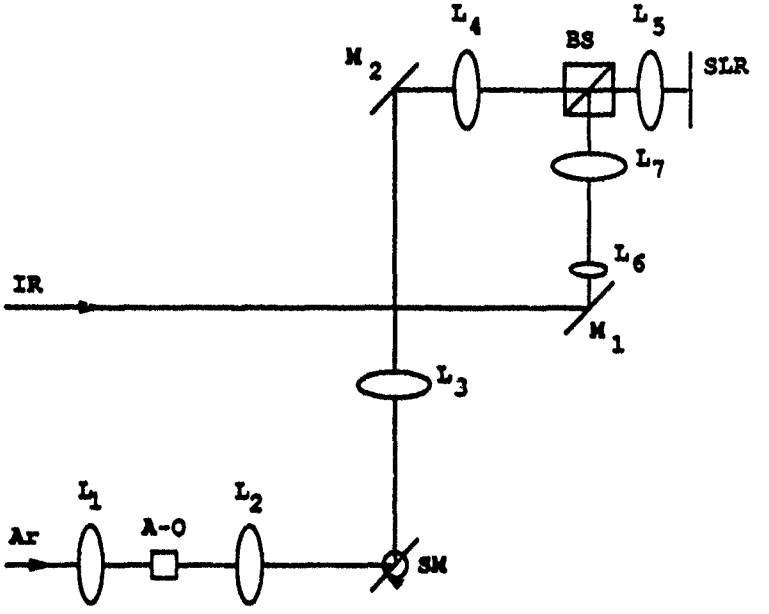

Figure 10: Optical set-up for scanning resolution experiment

row by row raster scan. Lens L_5, having a focal length of 35 mm, focuses the 3 mm diameter beam to a spot of approximately 6 μm.

The experimental result is shown in figure 11 for scanning with the thin film CaS sample. The acoustooptic cell was modulated at 10 kHz and the scanned area is 5 mm × 4 mm. The light dashes are therefore 100 μs long. The resulting resolution is approximately 25 line-pair/mm, equivalent to a spacing between lines of 40 μm.

3.2.3 Infrared modulation and diffusion

IR passes through an SLR more easily where no electrons have been trapped. In this case, the device acts as a spatial light modulator (SLM) and could perform a masking operation for selective memory reading. Figure 12 shows that, for a thick film, some of the energy in a 5 mm IR beam is transferred to luminescence causing a reduction in the infrared passing. The dash line corresponds to the infrared intensity passing through the thick film when no electrons are trapped. The solid line shows the intensity of the infrared passing through the material when electrons were trapped on the material. Note the large dynamic range over which modulation is effective.

Modulation is defined as:

$$M = \frac{I_{max} - I_{min}}{I_{max}} \tag{5}$$

where I_{max} is the output intensity in absence of trapped electrons, and I_{min} is the output intensity with trapped electrons. Modulation was calculated for the thick film

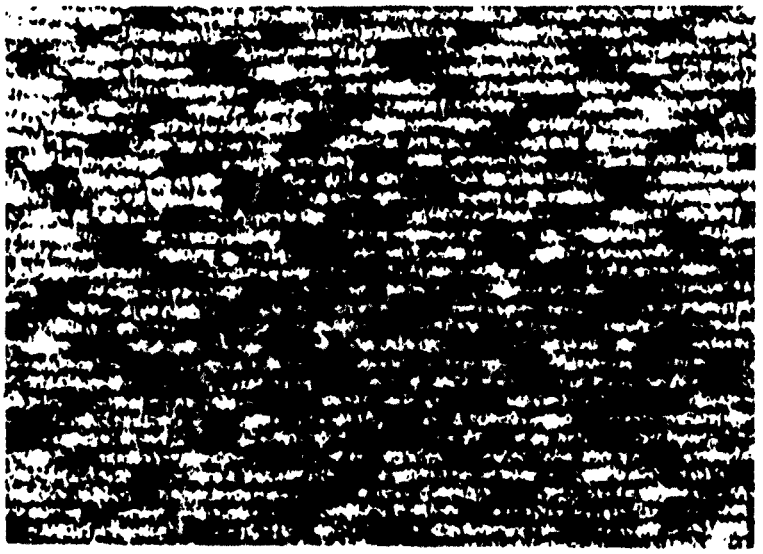

Figure 11: Result of scanning experiment shows resolution and speed

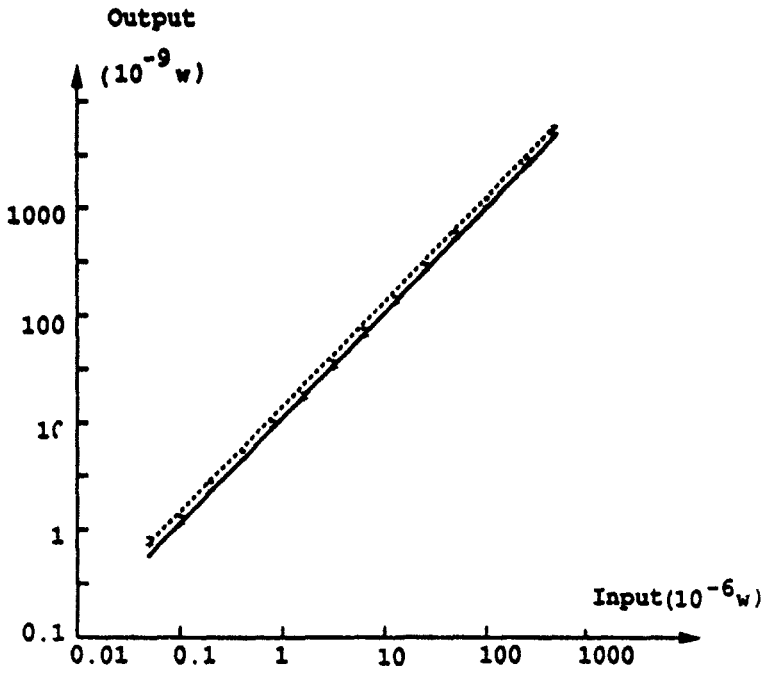

Figure 12: SLR infrared output versus input

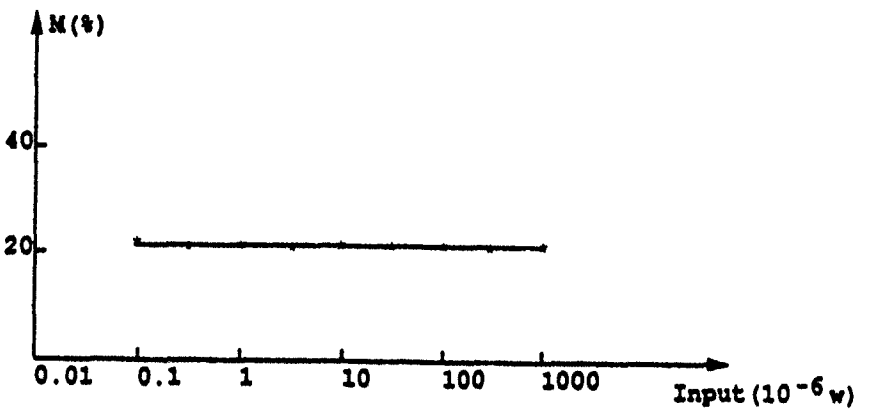

Figure 13: SLR infrared modulation

and the result is shown in figure 13.

Because the CaS SLRs are not transparent, they act as a diffuser. The distribution of intensity 13 mm behind the material is shown in figure 14. The dash line corresponds to thick material and the solid line to thin material. As expected, the thick film diffuses more than the thin film.

3.3 Performing logic with SLRs

A sequence of OR operations on a sequence of binary images A, B, C etc. is performed by writing one image after the other onto a device that was previously cleared by flooding with IR [52]. The stored energy may be written as:

$$S = A + B + C \cdots \tag{6}$$

On reading the device by flooding with IR, the intensity of the luminescence at a pixel represents the OR of the input binary images. If analog images are used in place of binary ones, and the intensity remains below saturation, the operation performed is the addition of analog images [52].

Parallel ANDing of binary images A and B is performed by writing one image, say A, onto the device with intensities that saturate the device and then reading with a binary IR image representing the second image B. The output luminescence at each pixel position, after scaling, is the AND of the read intensity at that pixel and the stored value at that pixel:

$$Out = A \cdot B \tag{7}$$

If analog images are used, and intensities remain below saturation, the operation performed is analog multiplication of images [52].

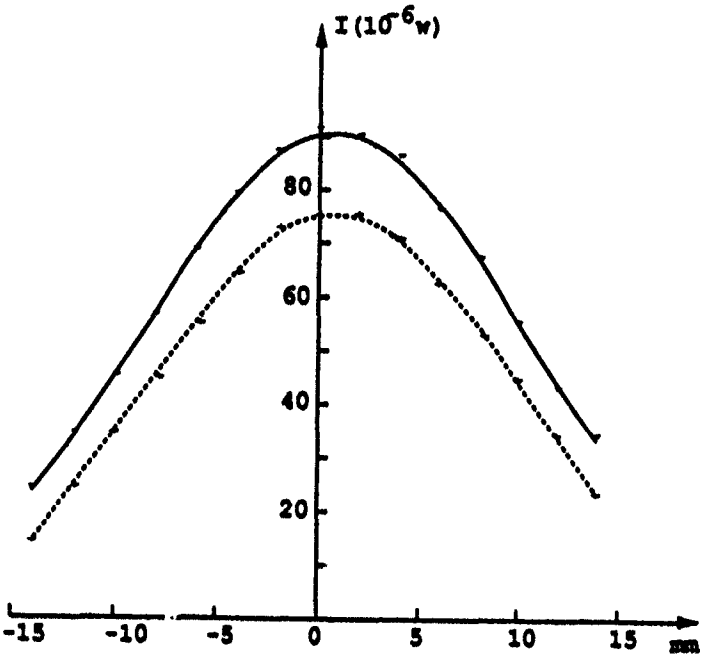

Figure 14: SLR infrared diffuser

The device can also perform a sequence of AND NOTs by writing an array of ones and then performing successive reads with binary arrays B,C,D, etc. The stored energy is

$$S = \overline{B} \cdot \overline{C} \cdot \overline{D} \cdot ..... \tag{8}$$

As $\overline{B} \cdot \overline{C}$ is equivalent to $\overline{B + C}$ or NOR, the system is capable of performing a sequence of NORs.

In some cases, the ability to perform alternative logic operations leads to more efficient implementation than using a simpler set. The 16 basic logic operations between two inputs [30] were performed using SLRs in reference [51].

4 Basic modules

Computers are constructed in a modular manner so that different technologies can evolve at different rates and without impacting software. Further, modules provide economies of manufacture. We suggest several modules using available optical components, including an SLR based cascadable module, template matcher, and correlator. These basic modules are used in section 5 for higher level computations.

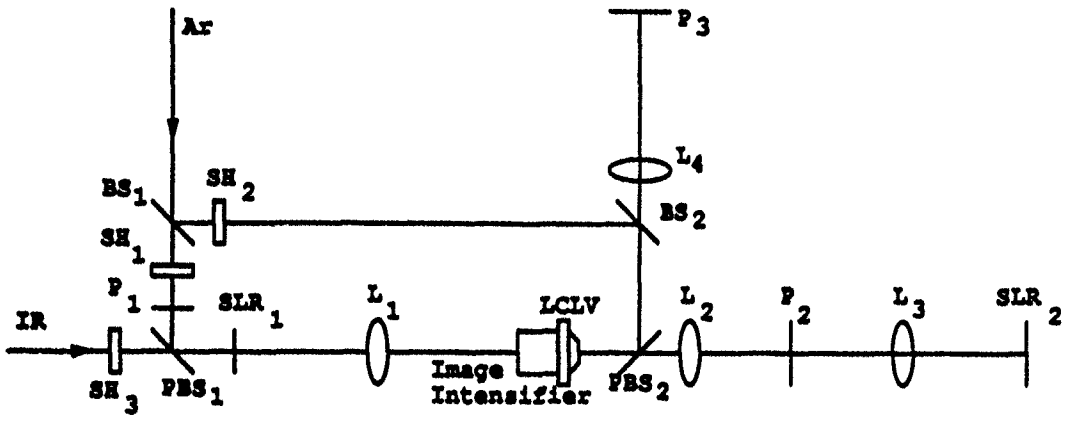

Figure 15: Optical set-up for cascadable optical module with SLR

4.1 Cascadable module using SLR

Synergistic devices may be combined with an SLR to overcome disadvantages of attenuation, incoherent output, and differing wavelengths at input and output [53]. The additional devices, an image intensifier, and a liquid crystal light valve, are characterized first.

4.1.1 Characteristics of other devices in module

A Ziemer XX 1420 L7811 image intensifier was illuminated with a Helium neon laser and the output intensity measured on a plane 8mm behind the image intensifier. The gain is approximately 960 over a wide range of inputs.

A Hughes OLCLV was driven with a 20 V 0.1 ms sine wave. Detectors were used immediately before and after the OLCLV to record the input and output intensity. Two sets of spatial filters and collimating lenses were used to generate plane waves. The laser, of wavelength 514 nm, was operated in feedback mode in order to obtain a stable laser output. A liquid crystal light valve that permits reading with IR is being developed by Hughes.

4.1.2 Experimental results for cascadable module

A module was created, as shown in figure 15, by feeding the output of SLR into an image intensifier and the output of the image intensifier into an optically addressable liquid crystal light valve (LCLV).

Figure 16(a) shows a 2-D binary pattern used for experiments. This pattern is

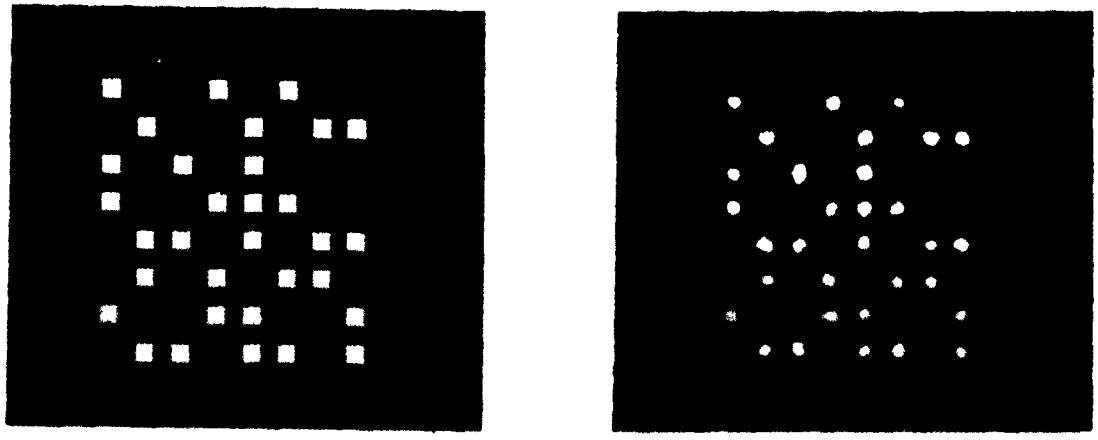

Figure 16: Optical module experiment (a) input, (b) output

placed at P_1 in figure 15. Argon light maps the pattern onto SLR_1 via beamsplitter BS_1, shutter SH_1 and polarizing beamsplitter PBS_1. Shutter SH_1 is then closed and shutter SH_2 and SH_3 are opened to allow light to pass. Infrared passes through shutter SH_3 to read SLR_1. The output passes through the image intensifier and writes on the photoconductive side of LCLV. Argon light, passing through SH_2 is polarized vertically, so that it reflects off PBS_2 onto the right face of LCLV. Any pixels for which the photoconductive side of LCLV were activated, will cause a 90° change in polarization of the light out of LCLV. This passes directly through PBS_2 because it is horizontally polarized. The image at LCLV is Fourier transformed by lens L_2, passes through a spatial filter P_2, which is a small spot to block low spatial frequencies, and is then inverse Fourier transformed by lens L_3. The result is that the image at LCLV is imaged onto SLR_2 while being low pass filtered.

The image at SLR_2 is shown in figure 16(b). The signal level at the output is sufficient to write on another device. The gain around the loop is approximately 1000 in the image intensifier and 30 in the OLCLV. This compensates for the loss in the SLR between write and output energy and the loss in the high pass filter.

4.1.3 Performing memory and logic with cascadable module

SLR_1 may be used as a memory for storing 2-D patterns. This provides a buffer mechanism for synchronizing when using several cascadable modules for computing more complicated functions.

The OR operation between **A** and **B** may be performed in figure 15 by setting **A** on an ESLM at P_1 and activating the Argon laser by opening shutter SH_1 for an instant. Then **B** is set on ELSM at P_1 and the shutter SH_1 is again opened for an instant. The OR of **A** and **B** is now stored on SLR_1. The arrays **A** and **B** may be

used simultaneously instead of separately. In this case, two optical binary arrays **A** and **B** are merged with a polarized beamsplitter to illuminate SLR_1. SH_2 and SH_3 are now opened and this causes infrared to image the OR pattern onto the image intensifier. The result is read off the right side of LCLV and imaged through the spatial filter onto SLR_2. The NOR output appears at P_3. A spatial filter was not needed for the NOR output.

The AND operation between **A** and **B** is performed by setting **A** in an ESLM at P_1 and opening SH_1 for an instant in order to image **A** onto SLR_1. Pattern **B** is now superimposed on the IR beam and shutter SH_3 opened. The final result is an AND output, written onto SLR_2. The NAND output appears at P_3. Subsequently, we show how to construct half and full adders using the cascadable module and a few additional components.

4.2 Template matching

Template matching, traditionally used in classification, is also important for memory addressing. In a RAM, the template can be a binary address, while in associative memory, they represent stored keyword references that are associated with output data. The matching is performed by taking an inner product between an input and each template.

Note that in a binary system, the matching performed verifies only that the position of '1's in the input agree with those of the matched template. The matching for '0's may be accomplished by complementing the templates, using dual-rail coding, or polarization. We consider 1-D and 2-D template matching separately.

4.2.1 1-D template matching

I-D template matching may be performed by binary matrix-vector computation. In addition to memory, other applications for binary matrix-vector multiplication include: crossbar switching, programmable logic arrays, and neural networks [48]. Previously analog matrix-vector multiplication was proposed for an ultrafast radar processor [49] and an expert system using Bayes theory [55].

The binary matrix is set on a spatial light modulator such that each pixel is either transparent, representing '1', or opaque, representing '0'. The input vector activates a 1-D array of LEDs or laser diodes. Lens systems are used to generate the results [48](Chapter 11). The output is thresholded if a binary output is required.

Figure 17 illustrates a 100 by 100 matrix-vector multiplication with an SLR, [51]. A binary matrix pattern was imaged from a piece of film onto the SLR. The matrix multiplies a binary vector to produce a resulting vector as shown.

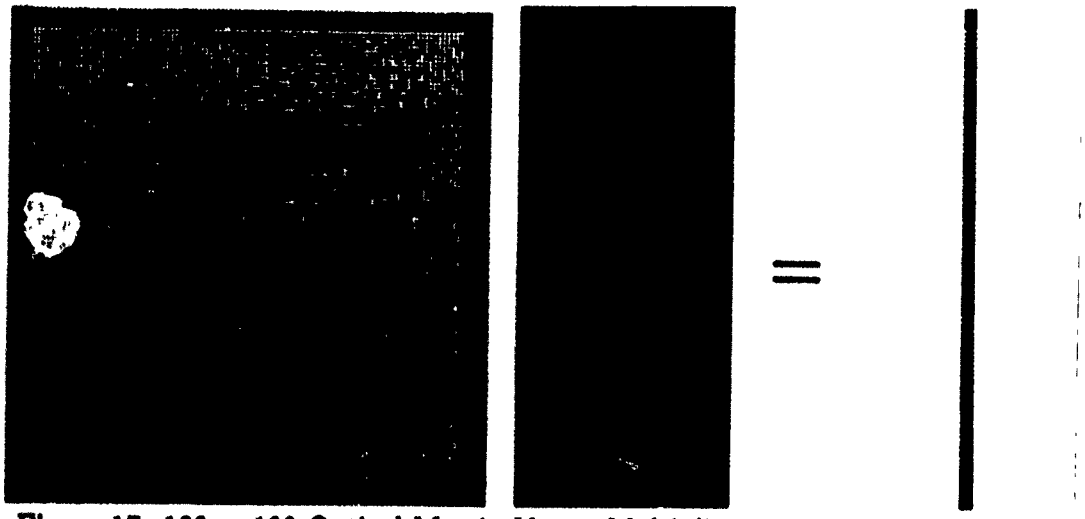

Figure 17: 100 × 100 Optical Matrix-Vector Multiplication Result with SLRs

4.2.2 2-D template matching

Matrix-vector multiplication involves inner products between an input vector and vector templates. If the templates are 2-D we can perform inner products of a 2-D input with 2-D templates. In this case, we need to replicate the input image by means of mirrors, lenslet arrays, crystals, or holograms. Shadow casting is an effective means of performing template matching in the space domain between the input and each stored template [30]. The computation performed is:

$$z = \sum_{i=1}^{n} \sum_{j=1}^{m} x_{i,j} y_{i,j} \tag{9}$$

Results for discrimination between X and O using this approach are shown in reference [54],[48](Section 5.3.5). In section 5.6 of this report, 2-D template matching is used in learning.

4.3 Binary correlators

In digital computing schemes, such as cellular automata and the search phase of symbolic substitution, we search for all occurrences of a pattern (or kernel) at unknown positions in a 2-D array. A correlator may be used, which involves repeated inner product computations as one of the images is shifted one pixel at a time. The operation may be regarded as space invariant filtering because the same spatially relative operation is applied to every element. Template matching, described previously, is sometimes referred to as zero shift correlation.

Figure 18: Experimental result for 4-f correlator: (a) orthogonal pattern, (b) output of correlator

4.3.1 Space domain correlator for simple kernels

A number of methods may be used for space domain correlation. If a filter or kernel has only n pixels set to '1', we need to replicate the input image n times. Mirrors, beamsplitters, or holograms may be used to replicate an image a number of times and shift them according to the positions of each pixel. The shifted replicas are then merged and an appropriate threshold applied. The threshold will be exceeded at those positions in the image for which every pixel is present at the correct relative position.

Pattern logic [74] is an efficient way to perform the space domain correlation operation. As an example, a four leaf orthogonal kernel is implemented by activating appropriate light sources in an array of four light emitting diodes (LEDs) or laser diodes [48](Section 8.3.3)). Each source projects a different image of a 2-D input array onto an output plane. A Fourier transform reduces the size so that each replica reflects from a different segment of a segmented mirror. Each segment of the mirror is angled so that, after inverse transforming, the resulting images are brought back together with the appropriate displacement of one row or column. For four light sources, a threshold close to four times the intensity of one source after passing through the system, ensures that all four orthogonal neighbors must be '1' in order for a pattern to be detected.

4.3.2 Correlators in the Fourier transform domain

A well known theorem in digital signal processing states that convolution in the space domain is equivalent to multiplication in the Fourier transform domain [61]. This may be implemented with an optical 4-f correlator as first proposed by Van der Lugt [75], [18].

Figure 18(a) shows a four leaf orthogonal pattern proposed for cellular automata computers [58]. Any occurrence of this pattern in an array will give rise to a correlation peak and a convolution peak on opposite sides of the center in a correlation

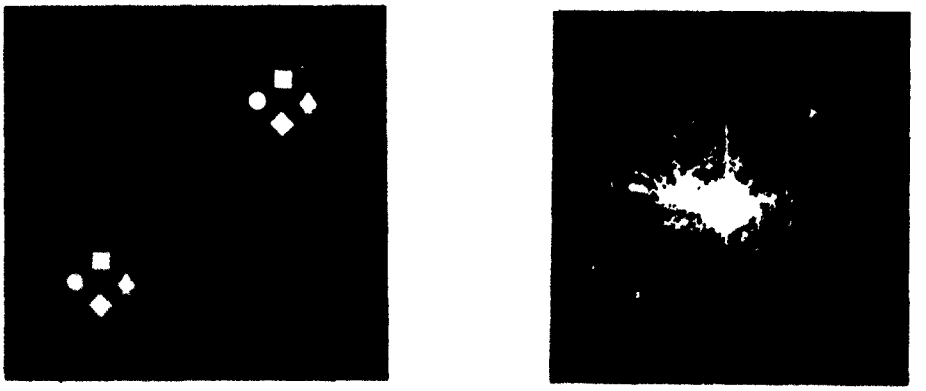

Figure 19: Experimental result for joint transform correlator: (a) orthogonal different patterns, (b) output plane

plane. We considered a single occurrence of the pattern and obtained the results shown in figure 18(b) showing the correlation and convolution peaks.

Joint transform correlators are an alternative implementation of correlation in the Fourier transform domain. They are of interest because the filter or search array can be dynamically varied more easily than in a 4-f correlator. In a 4-f system, the filter must have holographic resolution if phase and amplitude are to be stored. Phase only filters do not require such resolution because only phase is used in the filter, and they have negligible loss. In a joint correlator, both input data and filter are entered at the same 2-D input plane. The Fourier transform of the plane is taken and the result squared with a nonlinearity. We use a liquid crystal light valve for the nonlinearity in our experiments. The output of the liquid crystal light valve is inverse Fourier transformed to produce an output plane in which the correlation and convolution are included. In figure 19(a), we show an orthogonal pattern with different patterns in each leaf. Figure 19(b) shows the correlation dots at 45° showing correct recognition of the pattern. However, if the same pattern is used for each leaf, the dots are no longer visible because the joint transform correlator generates noise cross terms that are not produced in a 4-f correlator, and these noise terms remove energy from the desired dot positions. Increasing the intensity so as to move to the nonlinear part of the liquid crystal light valve input response can increase the correlation signal somewhat.

5 Computational modules

The basic modules of the last section are used with SLRs to investigate ease of constructing digital optical computer subsystems. We consider SLRs for two examples of heteroassociative memory modules in which the vector $\mathbf{x}_i$ is associated with the vector $\mathbf{y}_i$ for $i = 1$ to J. When queried with the vector $\mathbf{x}_i$ the memory responds

with the vector y_i. In the first memory, the input and output have similar bit length. In the second memory a large output is generated from a key word reference. This corresponds to a key word search for a page or more of data in an electronic database.

Two optical adders are considered using SLRs. Experimental results are presented for a parallel set of half adders that may have output and input connected to generate a parallel ripple carry adder. The second, a pipeline adder using cellular automata principles, was simulated on a computer.

The method of moving words around through optical interconnections in an all optical random access memory machine is described and experimental results shown. Finally the SLR is used to demonstrate optical learning using a Perceptron algorithm, modified for the positive nature of light intensity. The SLR is suitable because weights can be increased by writing and reduced by reading.

5.1 Optical heteroassociative memory using spatial light rebroadcasters

We describe optical learning and recall for an orthogonal heteroassociative memory [51].

5.1.1 Optical learning

Optical learning is accomplished by storing a number of associations by summing their outer products to form a matrix **A**. Figure 20 shows the optical set up for the generation of a 32-bit heteroassociative memory matrix. The Argon laser beam is collimated and focused by means of cylindrical lens S_1 onto one column of the film located in the plane labeled vector **y**. The column represents one of the output vectors, **y**, involved in the association. After passing through the vector **y** plane, the light spreads horizontally. There is a horizontal line of light corresponding to every clear spot, '1', in the column on the film representing vector **y**. A spherical lens L_1 focuses these lines on to one horizontal line in the plane labeled vector **x**. Film with the vector **x** to be associated with **y** is placed at this position. The light passing through the vector **x** expands vertically so as to produce the outer product of **x** and **y** at the spatial light rebroadcaster (SLR). Note that vertical columns are passed only where the vector **x** has '1's. The SLR stores this outer product.

The film at the position labeled vector **y** is moved horizontally in order to perform an outer product for another associated pair. The film at the position labeled vector **x** is moved vertically to provide the **x** that corresponds with the **y** selected. The resulting outer product for the new associated pair is stored on top of that previously stored on the SLR. The addition of many outer products form **A**. Binary, vector pairs were selected so that the resulting matrix has only '1's or '0'es, that is, remains

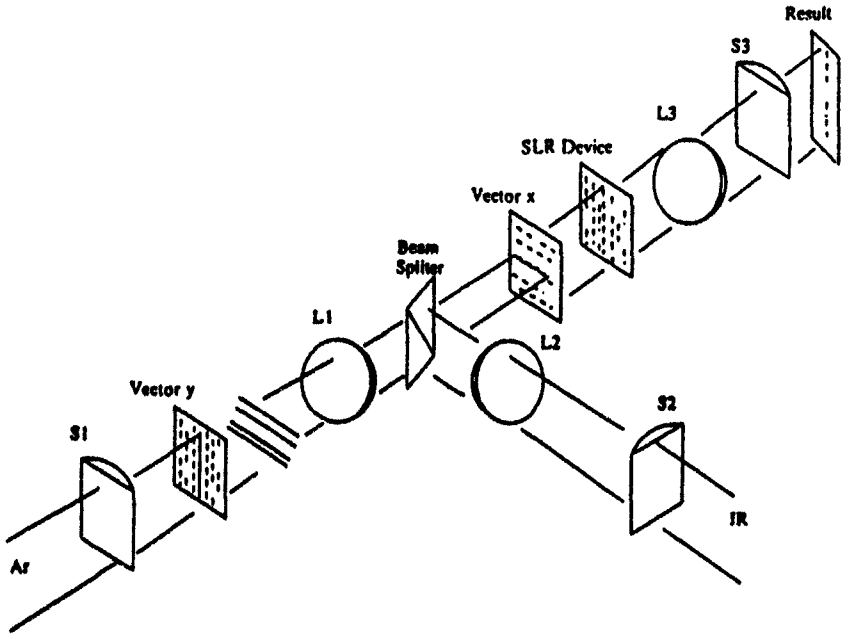

Figure 20: Optical set up for neural network associative memory with SLR device

binary. This is similar to the learnmatrix concept which is claimed to have highly efficient storage relative to other neural networks [22].

Figure 21(a) shows a matrix y whose 16 columns each represent one of the 40-bit output vectors. The input vectors corresponding to these outputs are the 16 32-bit rows in figure 21(b). The first column in figure 21(a) corresponds to the first row of figure 21(b) and so on. The two matrices were placed on film and the two figures were produced by shining collimated light through each film separately.

The y and x matrices were placed in the positions labeled vector y plane and vector x plane respectively in the optical set up shown in figure 20. The outer product was generated and stored as described previously by shifting the y horizontally and x vertically until the outer products for all 16 pairs were generated and stored on the SLR. The SLR was then illuminated to produce luminescence corresponding to the sum of the outer products and this was photographed to produce figure 21(c).

5.1.2 Memory recall

If the input vectors are orthogonal, $\mathbf{y}_i$ the association for $\mathbf{x}_i$, may be recovered by a simple matrix-vector multiplication [16], making use of the orthogonality assumption $\mathbf{x}_j^T\mathbf{x}_i = 1$ when $i = 1$, and 0 otherwise. This is illustrated by separating the ith term.

$$\mathbf{A}\mathbf{x}_i = \mathbf{y}_i(\mathbf{x}_i^T\mathbf{x}_i) + \sum_{j \neq i} \mathbf{y}_j(\mathbf{x}_j^T\mathbf{x}_i) = \mathbf{y}_i \tag{10}$$

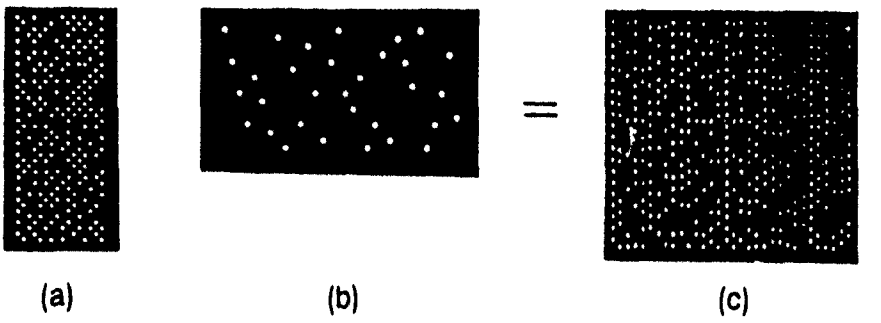

Figure 21: Experimental result of orthogonal neural network associative memory: (a) vector y, (b) vector $\mathbf{x}^T$, (c) associative memory matrix

In figure 20, the optical set up is arranged in such a way that the Argon laser and IR laser come from different angles, which reduces the complexity of the experimental procedure. The cylindrical lens S_2 and spherical lens L_2 act in the same manner as S_1 and L_1, except that the light is not modulated. They cause a single horizontal line to be illuminated in the plane labeled vector x. Film with the input vector x, whose association is sought, is placed at this row. The illumination is such that the light is spreading vertically to illuminate those columns of the SLR corresponding to positions in vector x that have '1's. The resulting luminescence is focussed in the vertical direction onto the plane labeled result by means of L_3 and S_3. The vector resulting from the matrix-vector multiplication is the output y associated with the input x.

The results are illustrated in figure 22. The associative memory, stored as the sum of outer product matrices in an SLR, is shown in figure 22(a). Figure 22(b) shows the film used with 16 input vectors arranged as columns. This film is placed at position labeled vector x in figure 20 such that the vectors are horizontal. One of the columns labeled p, q, or r, in figure 22(b) is placed at the active row position in the optical set up. The corresponding output, obtained at the result position in figure 20, was photographed. The sixth column in figure 22(b) is labeled p. It has a '1' in the tenth entry from the top and no other '1's. Hence, on premultiplying by the matrix, this should result in the selection of the tenth column of the matrix in figure 22(a), as shown in figure 22(c). Similarly, q has a '1' in position six and r a '1' in position seven. This leads to the sixth and seventh columns of the matrix being selected as shown in figure 22(d) and (e) respectively.

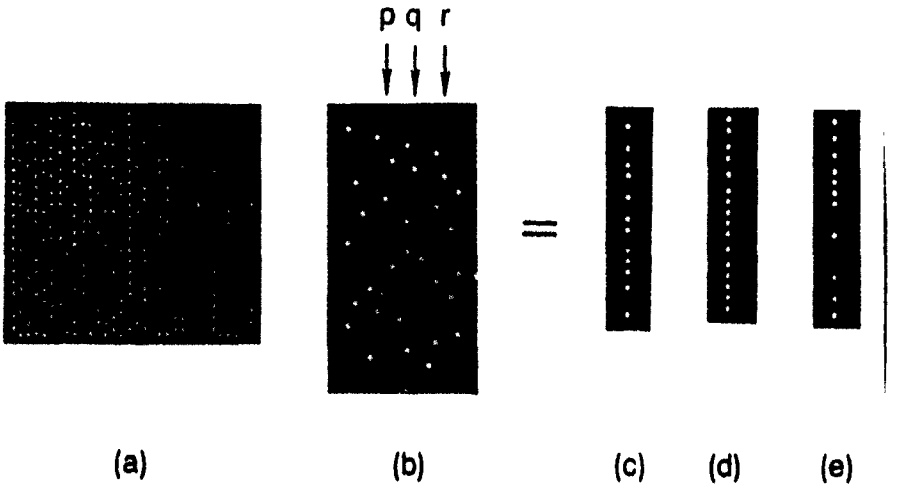

Figure 22: Recall from associative memory for three different input vectors: (a) stored outer product matrix, (b) array containing input vectors p, q, r, (c) output vector corresponding to p, (d) output vector corresponding to q, (e) output vector corresponding to r

5.2 Spatial light rebroadcaster bit-slice word-addressable holographic memory

The previously described heteroassociative memory has outputs of similar size to inputs. In this section, a key word is used to select a holographic image with over 40,000 bits as shown in figure 23 [53].

Optical bit-slice search

A *bit-slice search and replacement* [48], invented on this project, avoids the difficulty of implementing a winner-take-all circuit needed in making a decision for template matching. It differs from symbolic substitution in two ways. First, it permits the search word to be entered serially, which is more suitable for interfacing with electronics. Second, it requires less powerful sources because only 1-D illumination is used instead of 2-D.

Figure 24 shows the optical set up for performing bit-slice search. A database of key words, as shown in figure 16(a), is written using blue laser light onto the spatial light rebroadcaster, SLR_2, where each key word occupies a row. The complement of the database is written onto SLR_1.

The key word, whose association is sought, is entered onto the electronically addressable spatial light modulator $ESLM_2$, and its complement on $ESLM_1$. Collimated infrared light is introduced at CL_1. The input beam has a vertical spread, and

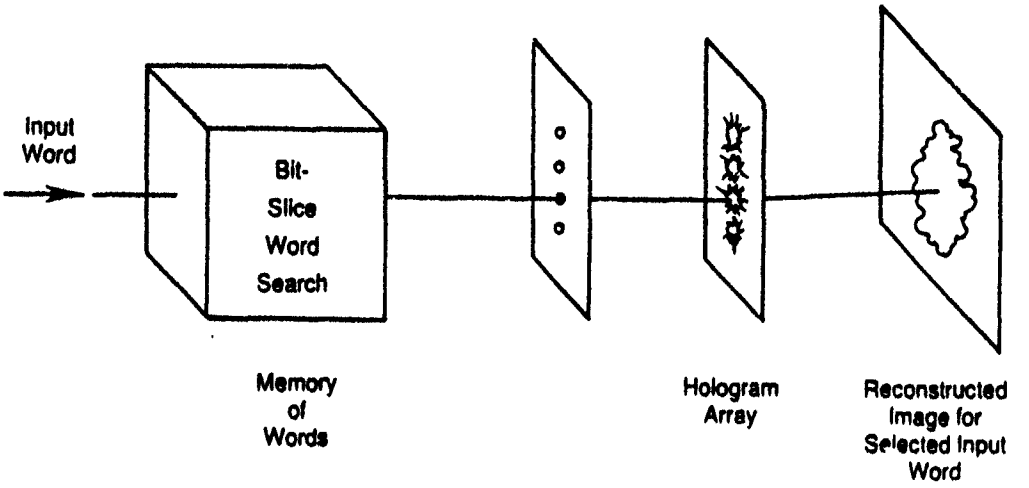

Figure 23: Associating key words and holograms

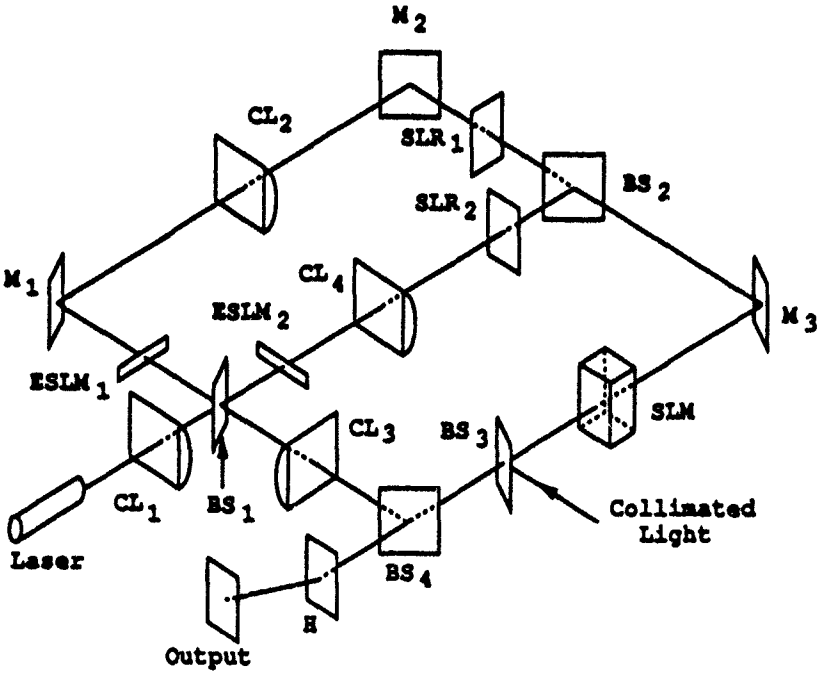

Figure 24: Optical set up for bit-slice search of key word

in the horizontal direction it is narrow and in alignment with the left most pixel of $ESLM_2$.

If the leftmost pixel of $ESLM_2$ is set clear, after passing through $ESLM_2$, the beam expands in the vertical direction and is then collimated by CL_4. On striking the spatial light rebroadcaster SLR_2, orange luminescence is generated at any point in the leftmost column that has stored data. This column vector of light is imaged onto an optically addressable spatial light modulator SLM. Mirror M_3 is set so that the vertical column is moved one column to the right of the normal alignment. Coherent infrared light is reflected off beamsplitter BS_3 onto the front face of the SLM. The reflected energy now provides a coherent replica of the column vector in infrared, which is needed for further loops. Cylindrical lens CL_3 focuses the light onto the second leftmost pixel of $ESLM_2$. In cases where a pixel on $ESLM_2$ is opaque, the corresponding pixel on $ESLM_1$ will be clear so that the complement is checked for matching.

The loop is repeated until light reaches the rightmost column in the feedback path. Only those rows of the database that exactly match the incoming key word will have light in the last column at the right on the final feedback loop. By choosing unique key words there will be only one spot of light in the rightmost column. The position of the spot in the vertical vector represents the number of the row corresponding to the matched word. The single beam illuminates one of a number of holograms at H to provide reconstruction of the associated image at the output.

Optical results

In an optical experiment, film is used in place of the SLRs because LCLVs cannot be read out with IR at this time as is required for looping. The second row of the database, figure 16(a), was used as the desired key word.

Eight images are stored as holograms on a piece of film. Each hologram is approximately one mm in diameter and the holograms are stored one under the other in a column. For simplicity of experimentation, this arrangement of holograms was chosen instead of placing the holograms on top of each other and addressing them at different angles. The film with holograms is placed at H in figure 24. The holograms show up as dark spots in figure 25(a), which was obtained by looking back from the position of H in figure 24. The light spots in figure 25 show the matching between the input word and the word database (figure 16) as the loop in figure 24 is traversed seven times during the bit-slice search. On each loop, the output was displaced one column to the right. The result in figure 25 shows that the key word matches rows 2, 5, 6, and 8 of the database for the first two bits at the left. This can be verified by inspection of figure 16. At the third loop, only the words in row 2 and 6 match the key word. After seven loops, only the second row of the database still matches the input keyword, so that only the second hologram from the top is illuminated. The reconstructed image from the second hologram is shown in figure 25(b).

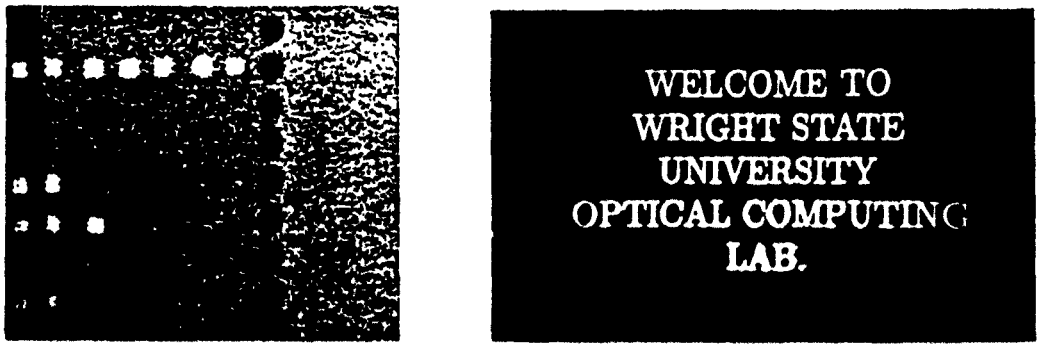

(a) (b)

Figure 25: Bit-slice search experiment: (a) output pattern, (b) reconstructed hologram

5.3 Optical adder using spatial light rebroadcasters

The basic cascadable module of section 4.1 is used to construct a parallel half adder [47],[46]. A ripple-carry full adder is then described that uses the half adder with feedback.

5.3.1 Optical parallel half adders

We wish to compute the half adder for each pixel **A** with the corresponding pixel of **B**. The carry $\mathbf{A} \cdot \mathbf{B}$ is computed first using equation (1). At the same time $\overline{\mathbf{A} \cdot \mathbf{B}}$ is generated. This is split and one path is multiplied by **A** and the other by **B**. The result produces the *sum* from:

$$(\overline{\mathbf{A} \cdot \mathbf{B}})\mathbf{A} + (\overline{\mathbf{A} \cdot \mathbf{B}})\mathbf{B} = \overline{\mathbf{A}} \cdot \mathbf{B} + \mathbf{A} \cdot \overline{\mathbf{B}} = \mathbf{A} \oplus \mathbf{B} \qquad (11)$$

The array **A** is entered onto electronically addressable spatial light modulators, (ESLMs), at planes P_A and $P_{A'}$ in figure 26. The array **B** is entered onto electronically settable spatial light rebroadcasters at planes P_B and $P_{B'}$. We used film in place of ESLMs in our experiments. Operation proceeds by closing shutter SH_2 and opening shutter SH_1 in order to allow blue light to map pattern **A** onto the spatial light rebroadcaster SLR via beamsplitter BS_2. Shutter SH_1 is now closed and shutter SH_2 opened. Infrared from a Nd:YAG laser images the pattern **B** onto SLR. This generates orange luminescence out of SLR that is the AND of the two arrays **A** and **B**, pixel by pixel. The SLR, lens L_1, image intensifier Im_1, and LCLV, form a cascadable module (section 4.1. Blue light from the Argon laser illuminates the right side of LCLV via beamsplitters BS_1 and BS_3, and polarizing beamsplitter PBS. Pixels on the LCLV that were illuminated on the photoconductive side cause a 90^0 shift in polarization so that the blue light reflecting from the LCLV passes straight through PBS to plane P_1. Therefore, the carry output $\mathbf{A} \cdot \mathbf{B}$ is at P_1.

At the same time those pixels on the photoconductive side of LCLV that were not activated, do not change the polarization of the blue light so they will reflect

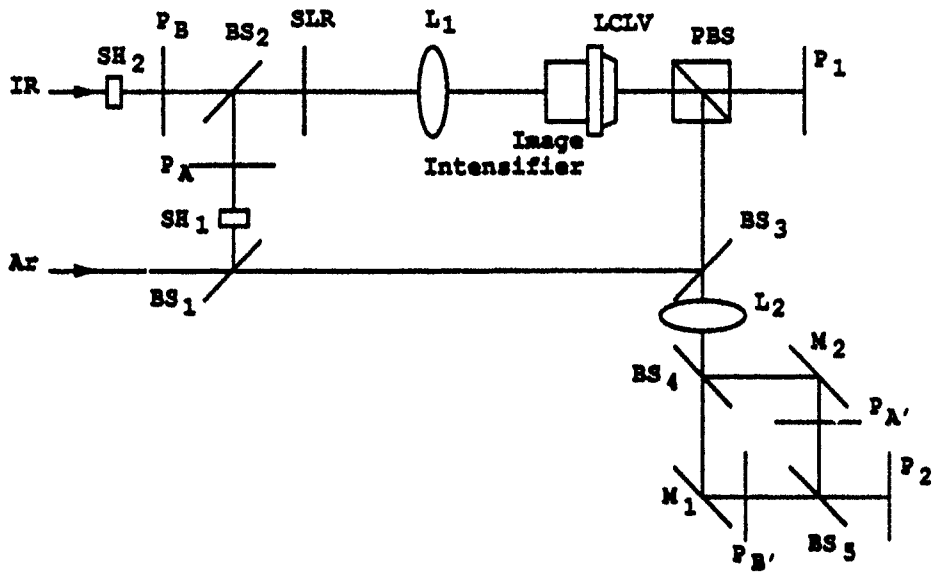

Figure 26: Optical set up for half adder

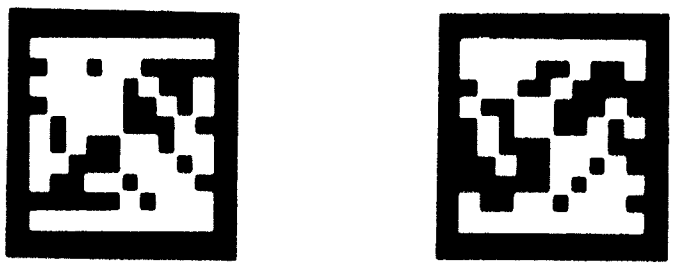

Figure 27: Input patterns for half adder experiment: (a) **A**, (b) **B**

from LCLV and then from PBS. BS_4 splits the beam into two directions, one passing through $P_{A'}$ and one through $P_{B'}$. The outputs are ORed to produce the *sum* term $\mathbf{A} \oplus \mathbf{B}$ at output P_2.

The input patterns **A** and **B** which were used for experiments are shown in figure 27(a) and figure 27(b) respectively. The light areas represent '1's and the dark areas '0's. The correct carry output, $\mathbf{A} \cdot \mathbf{B}$, at plane P_1, is shown in figure 28(a). The correct sum output, $\mathbf{A} \oplus \mathbf{B}$, at plane P_2, is shown in figure 28(b).

5.3.2 Optical ripple-carry full adder

We wish to add, in parallel, a number of words arranegd by rows in an **A** array to a number of similarly arranged words in a **B** array, where the words to be added are

(a) (b)

Figure 28: Output for half adder experiment: (a) carry, (b) sum

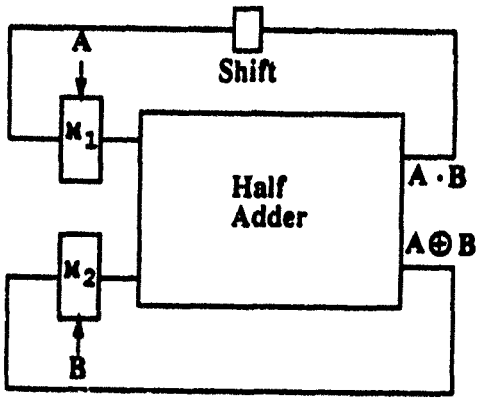

Figure 29: Parallel ripple-carry full adder

in identical positions on the two arrays. A parallel ripple-carry full adder is formed by feeding back the output of the half adder to its inputs as shown in figure 29. The loop is exercised six times for 6-bit words in order to propagate the carry from the least significant bit to the most significant bit.

A proposed optical set-up corresponding to the diagram in figure 29 is shown in figure 30. The half adder is shown in a dotted box and corresponds to the half adder set-up in figure 26. The outputs of the half adder are the carry at the output leading to SLR_2 at the top right of the dashed box, and the sum at the output leading to SLR_1 at the bottom left of the dashed box. Pattern **A** and pattern **B** are written on SLR_1 and SLR_2 respectively. Shutter SH_1 is opened, causing infrared to illuminate the SLR_1-SLM_1 module. SH_2 is opened at the same time and reads out the module causing the pattern **A** to be imaged to SLR_4 and SLR_5. Shutters SH_3 and SH_4 are now opened, causing **B** to be imaged onto SLR_3 and SLR_6 in a similar manner.

Shutters SH_5, SH_6, SH_7, SH_8, and SH_9 are now opened. These have the following effects. SH_6 causes an infrared read out of the **B** on the SLR_3-SLM_3 module and the resulting imaging of **B** onto SLR_4. The resulting carry $\mathbf{A} \cdot \mathbf{B}$ is stored on SLR_2 as a result of the opening of shutters SH_7 and SH_8. The alignment is such that it is stored shifted left one column so that the carry will be ready for inclusion with the next most significant bit on the next iteration. At the same time the inverse of the

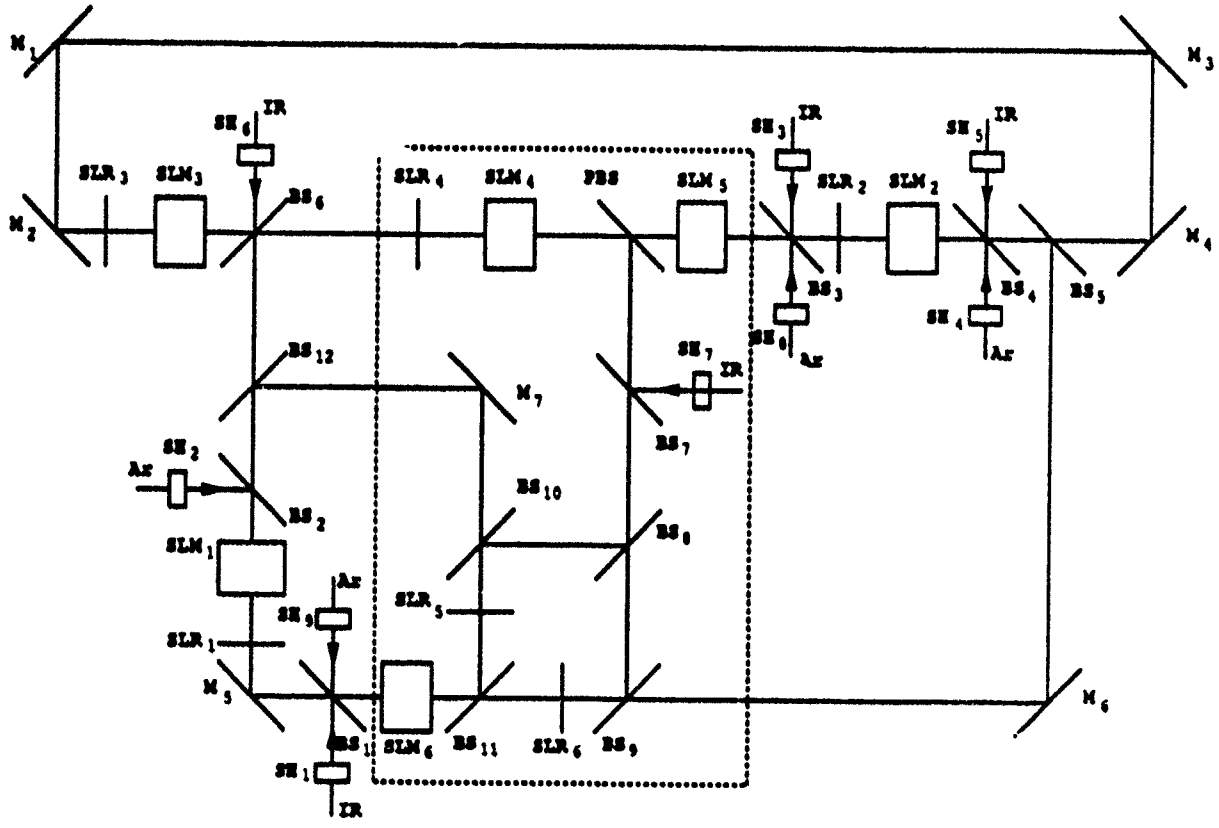

Figure 30: Optical set up for a parallel ripple-carry full adder

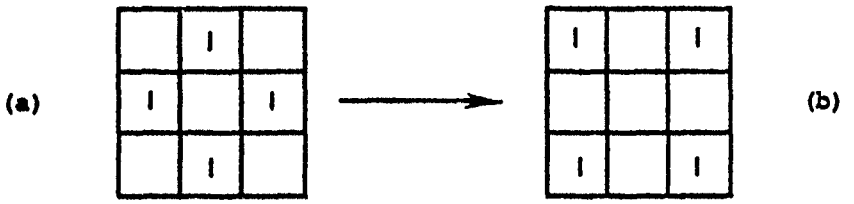

Figure 31: Nearest Neighbor Symbolic Substitution Rule: (a) search pattern, (b) substitution pattern

carry $\overline{\mathbf{A} \cdot \mathbf{B}}$ is imaged onto SLR_5 and SLR_6. This causes the exclusive OR output as described in the half adder equations (11). The sum is stored at SLR_1 as a result of opening the shutter SH_9. Consequently, a complete loop has been performed and the original **A** and **B** have been replaced by the outputs of the half adder, sum and carry respectively, ready for the next loop.

5.4 Optical adder using cellular automata

For high speed, high resolution devices, with several million pixels, it is impractical to control each pixel separately. The computation of control signals and their distribution would be more extensive than that for the computation being performed. One advantage of using cellular automata [48](Chapter 15), is that the same shift invariant operation is performed relatively on every element of a 2-D array.

5.4.1 Approach taken for simulation

In cellular automata, a cell is set to '1' or '0', based on the settings of it neighborhood. In a specific space invariant transition rule [59], the four diagonal nearest neighbors 31(b) are set to '1' if the four orthogonal nearest neighbors 31(a) are '1'. This configuration enables all the constructs required for computing.

Propagation is accomplished by presetting a path with '1's for the signal S to travel along, figure 32(a). S represents the signal and has value '1'. The path for the signal is set to include sets of three '1's positioned so that a further '1' at the left will provide a match and activate the rule. In this case, the path is fixed, while the cells set by the signal S will be erased if the rule is not satisfied on a subsequent iteration. The signal enters at the left and propagates across the array in three steps as shown.

Forks, merges, and crossovers are also demonstrated in reference [59]. Logical operations may be performed. Figure 32(b) shows a logical AND with a merge. Only if there are two signals entering at the top will there be an output at the bottom. This arises because the cell four across and three down will not satisfy the rule unless both sides are supplied with a signal.

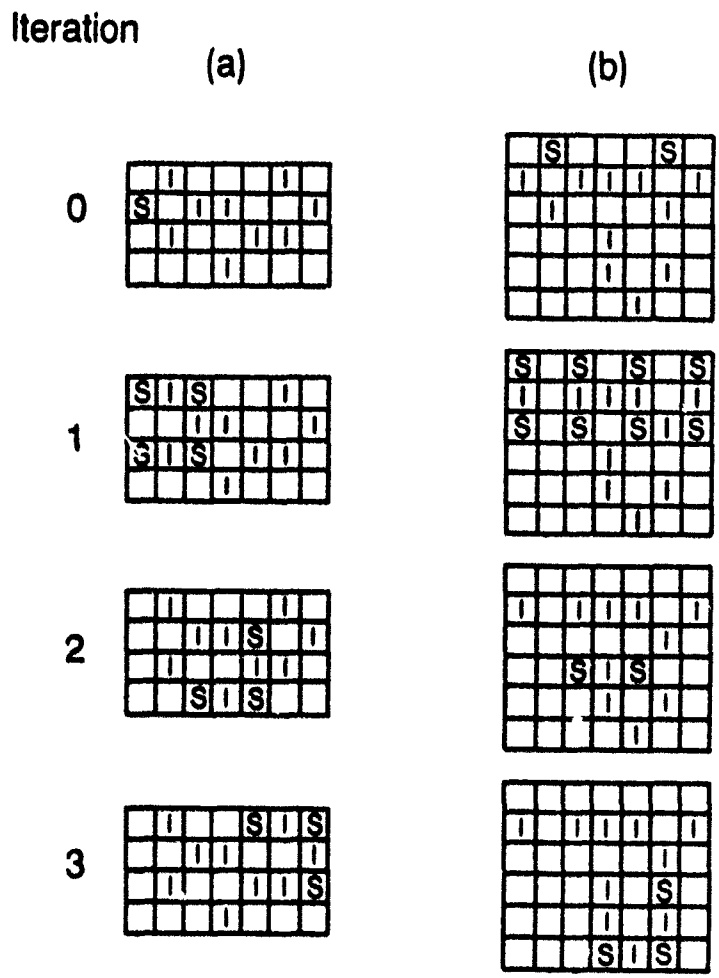

Figure 32: Computing with Nearest Neighbor Symbolic Substitution Rule: (a) Propagation, (b) Logical *AND*

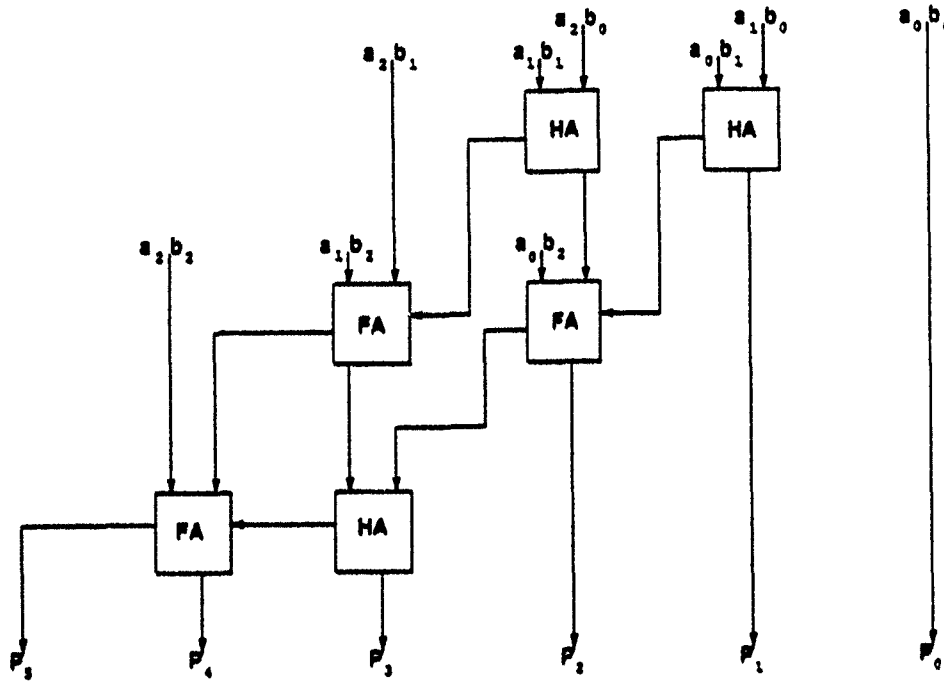

Figure 33: Logic diagram for three-bit multiplier

5.4.2 Simulation of three-bit multiplier

We performed a computer simulation to investigate the efficiency of this approach [68]. The simulation experiment determines the size of SLM and depth of pipeline needed for a three-bit multiplier. The multiplier provides a solution every clock cycle. Figure 33 shows the logic diagram for a proposed three-bit multiplier. The input words are a = (a_2, a_1, a_0) and b = (b_2, b_1, b_0), where subscript '0' represents the least significant bit. HA and FA stand for half adder, equation (1), and full adder 2 3 respectively. The output is p = $(p_5, p_4, p_3, p_2, p_1, p_0)$. As seen, a_0 is ANDed with b_0 to produce p_0. a_1 AND b_0 and a_0 AND b_1 are input to a half adder to produce the sum p_1 that passes to an output and the carry c_1 that passes to a full adder.

The cellular automata corresponding to the previous logic diagram for the three-bit multiplier has fixed points set to '1', marked by black dots in figure 34. In order to simplify the display, only the logic operations are shown. The movement of outputs between logic operations is omitted and replaced by a blank column. The complements of the outputs are also computed. There are nine boxes corresponding to the nine inputs in figure 34. Full adders are used, even when only a half adder was called for, in order to reduce the number of different patterns. After the AND operation in the first pattern column, the outputs enter the full adders. In order to see what is happening, figure 35 shows a cellular automata for a full adder satisfying equations (2) and (3). The left hand side performs the exclusive OR in the first pattern using $a \oplus b = a \cdot \overline{b} + \overline{a} \cdot b$. The second XOR operation in equation (2) is

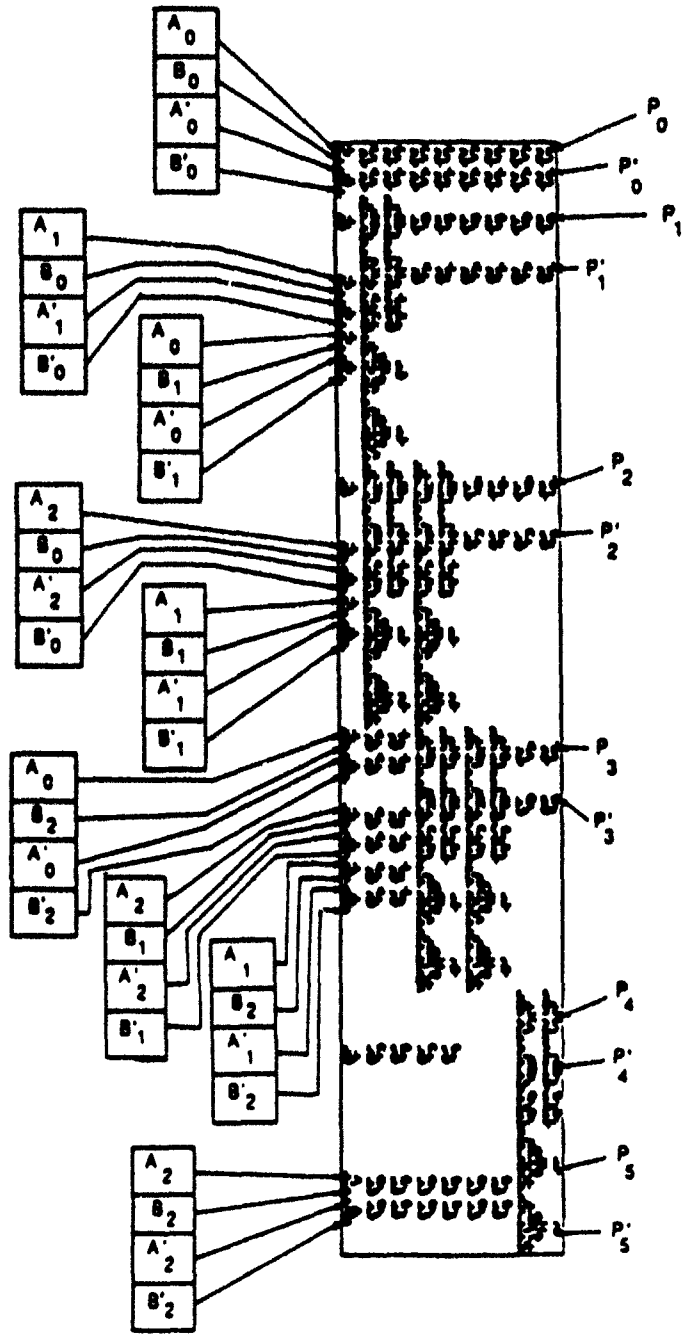

Figure 34: Three-bit cellular automata

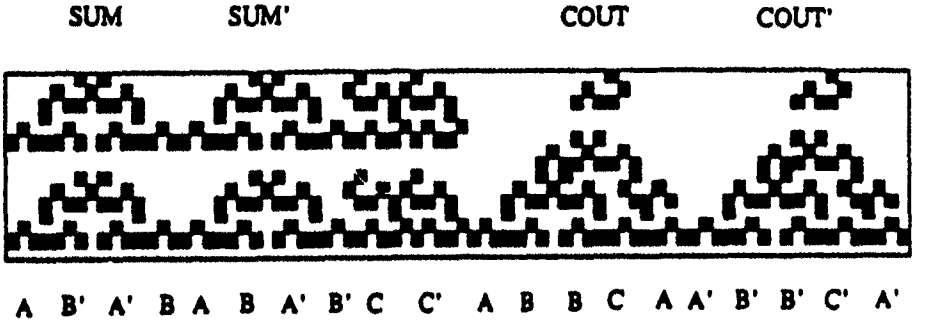

Figure 35: Cellular automata for full adder

performed in the second level. The carry and its complement are computed at the right side according to equation (3).

The results of the simulation show that 500 columns by 350 rows are needed in figure 34 for a three bit multiplier. The pipeline time is 250, so that 250 multiplications must be performed in sequence to fill the pipeline. These are preliminary results and it is likely that much smaller arrays and pipelines are feasible if more research is performed.

Any of the correlator methods in section 4.3 may be used for the search or recognition phase of the transition rule. A threshold is then used, for example on figure 18(b), and the resulting points spread, using mirrors or a single hologram in the Fourier transform domain, to the points shown in figure 31.

5.5 Optical interconnections for optical random access memory

An advantage of using an optical architecture that uses random access memory is that software developed for a sequential electronic machine is easily transferred to the optical machine because the same instruction set may be used. In the first optical computers, this advantage may outweigh inefficient use of optical parallelism. An architecture is proposed for the first time in reference [48](Chapter 13). The following discusses how data is moved from an address in one storage element to addresses in other storage elements.

An optical set-up is shown in figure 36. The data is stored as binary words in rows on material P_2. A horizontal slit on mask P_1 is imaged onto device P_2. The height of the slit at P_2 is set by the angle of mirror M. Instead of a mirror, a bit-slice

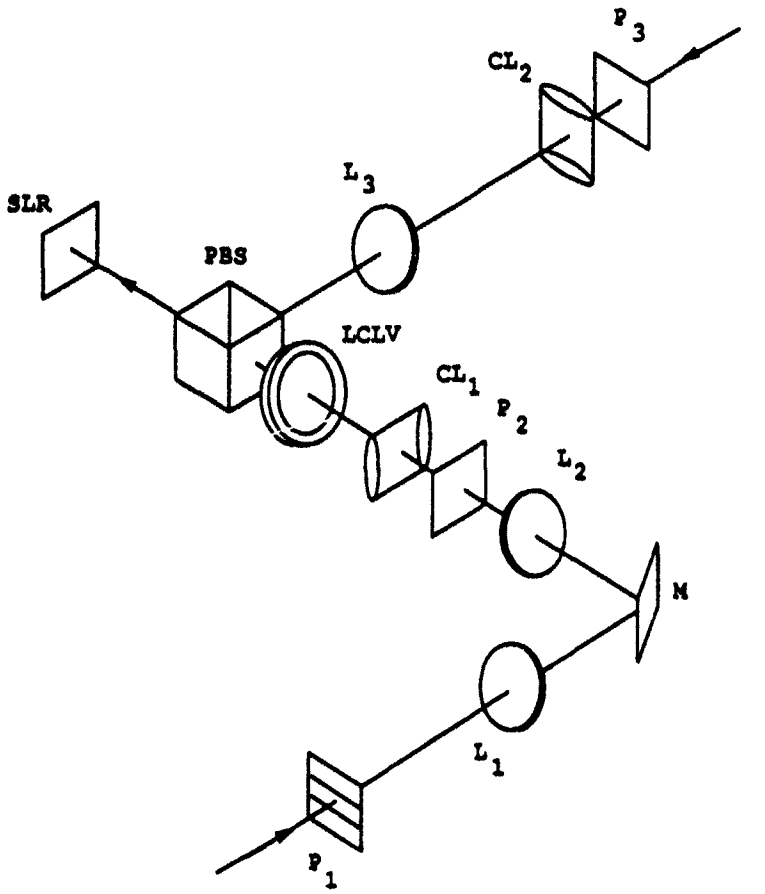

Figure 36: Optical set-up for optical random access memory interconnection experiment

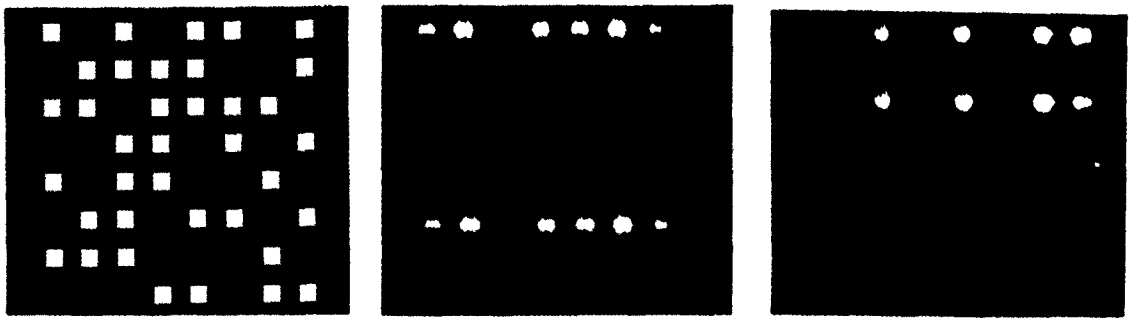

(a) (b) (c)

Figure 37: Interconnection experiment for RAM: (a) input words, (b) result of moving third row to first and sixth, (c) result of moving fourth row to first and third rows

approach [53] (section 5.2) could be used to set the height of the slit at P_2 according to an address. The selected word is spread vertically over the LCLV by lens CL_1. The address into which the word is to be placed on the final output SLR, is used to set the height of the beam entering P_3 using the bit slice technique (section 5.2). Lens CL_2 spreads the light across a row while imaging in the vertical direction onto SLR via polarizing beam splitter PBS. In the case of fanout, two output address beams are needed to read the LCLV out into two levels at the SLR.

Figure 37(a) shows an input set of binary words arranged in rows. We wish to move the third row to the first and sixth row positions on the output SLR. The result of the experiment is shown in figure 37(b). Moving the fourth row of the input to the first and third row of the output is shown in figure 37(c).

5.6 Learning with SLRs

SLRs are suited to neural network learning because a large number of weights may be separately increased or decreased in parallel. A variation of the Perceptron algorithm is used to demonstrate optical learning [50].

5.6.1 Optical Perceptron learning

The Perceptron algorithm [48](Chapter 12) is modified to operate with positive values for optics. In the modified Perceptron algorithm, for an incoming vector $\mathbf{x} = (x_1, x_2, \cdots x_n)$, the weights at the $(k+1)$th iteration are obtained from those at the (k)th iteration from:

$$\mathbf{w}(k+1) = \mathbf{w}(k) + \mu \begin{cases} 0 & \text{if } \mathbf{w}^T\mathbf{y} > e \\ \mathbf{y} & \text{if } \mathbf{w}^T\mathbf{y} < e \end{cases} \tag{12}$$

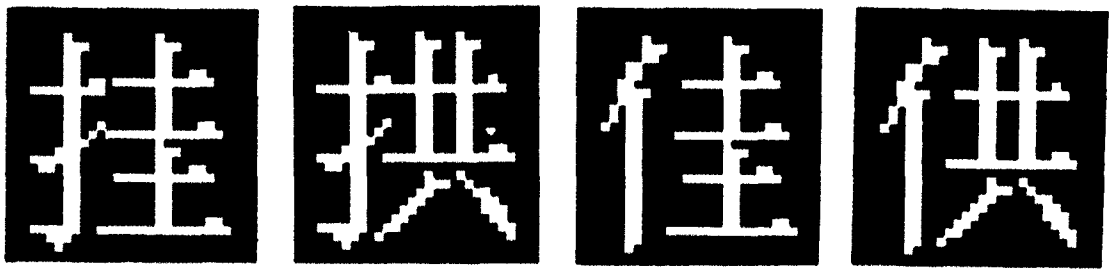

(a) (b) (c) (d)

Figure 38: Patterns used for optical learning demonstration: (a) Hang, (b) Arch, (c) Good, (d) Offer

where:

$$\mathbf{y} = \begin{cases} \mathbf{x} & \text{if } \mathbf{x} \text{ in class } C_1 \\ -\mathbf{x} & \text{if } \mathbf{x} \text{ in class } C_2. \end{cases} \tag{13}$$

Note that no change in weights is made if the top alternative condition applies in equation (12) because the classification is correct. The bottom alternative condition corresponds to incorrect classification and a weight change is made. The modification, relative to a Perceptron algorithm, is that the incoming data is not augmented by adding a '1' to the vector, a threshold e is used in place of '0', and the weights are constrained to be positive. It can be shown that this version of the Perceptron algorithm converges under certain additional constraints.

5.6.2 Optical learning experiment

We performed an experiment using an SLR to demonstrate the correct convergence of this algorithm for a simple case. Four binary chinese characters were used as shown in Fig. 38. Much simpler patterns were used earlier for optical demonstrations of Perceptron learning using photorefractive crystals [64]and SLRs [50]. It is simpler to use an SLR than a photorefractive crystal for this application. We wish to classify patterns (a) and (b) as class C_1 and patterns (c) and (d) as class C_2.

Fig. 39 shows an optical set up. The computer controls shutters for timing writing and reading onto the *SLR*. We start by writing a '0.1' over the SLR, as shown in figure 40(a). Then we set pattern (a) on ESLM. This pattern is multiplied pixel by pixel by the weights on *SLR*. The lens L integrates the array information spatially to a detector. This performs the inner product computation between the weights and the input vector $\mathbf{w}^T\mathbf{x}$. The computer reads the detector. If the output is correct during training, the computer controls the write shutter to open only long enough to

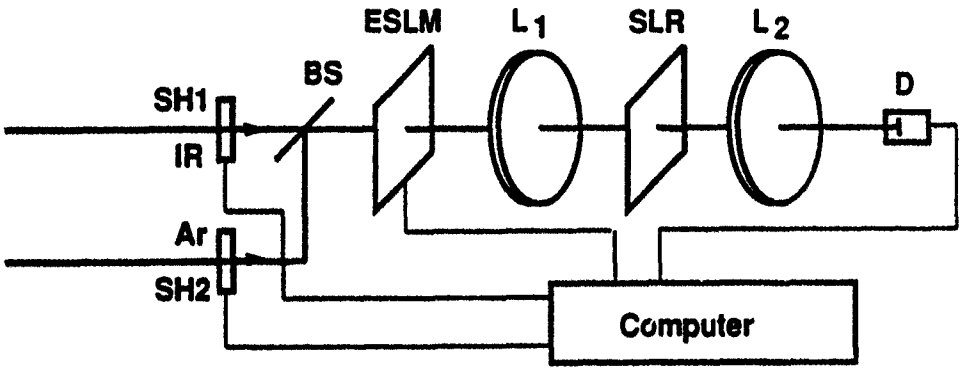

Figure 39: Optical set up for binary classification experiment

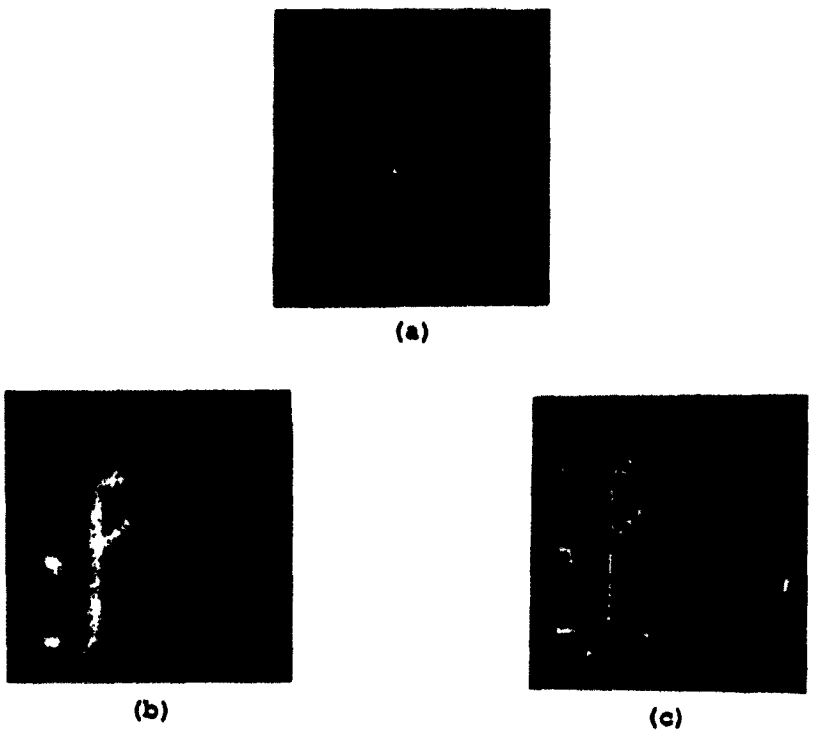

Figure 40: Weight patterns for optical learning: (a) starting pattern, (b) final pattern for thick film, (c) final pattern for thin film

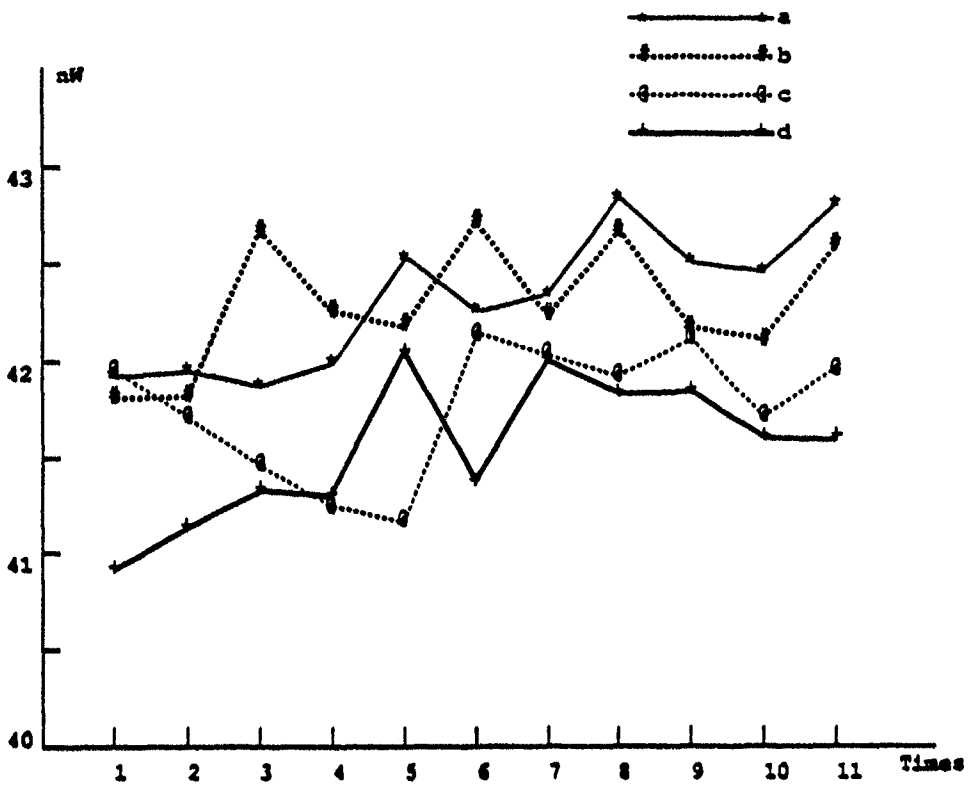

Figure 41: Learning curve for optical learning

compensate for energy lost from the SLR during read. This corresponds to no change in the algorithm, equation (12). If the detector output is opposite to that desired during training for class one, then the computer opens the write shutter for a longer time in order to add information selectively on the SLR. If the detector output is opposite to that desired during training for class two, then the computer opens the read shutter to remove some of the information selectively on the SLR. The computer rotates through all the patterns until there are no more changes in the weights stored on the SLR. The learning curve is shown in Fig. 41 after 10 cycles through all the patterns.

As a result of this training, if one of the input patterns is set on ESLM, the correct output will be seen at the detector. For example, (a) and (b) give a high output, indicating class one and (c) and (d) give a low output, indicating class two. The final weight pattern on the SLR for the thick film and the thin film are shown in figure 40(b) and (c) respectively. Note that it has weights equal to '1' in regions at the left where patterns (a) and (b) have '1' but patterns (c) and (d) have '0'. Therefore, when an inner product is taken between pattern (a) or (b) with the weight pattern, a high results. When an inner product is computed between the weight matrix and pattern (c) or (d), a zero results.

The system described uses a computer to perform thresholding. This is not a

bottleneck in the system described because the optics performs a 2-D inner product while only a single number needs to be thresholded. However, for multiple outputs and higher speed, an optical loop may be constructed by thresholding with an optical device such as a microchannel spatial light modulator [48](Chapter 5) or a liquid crystal with an improved threshold.

6 Future

We discuss the future development of SLRs and their application to optical digital computing.

6.1 Future development of SLRs

For use in digital optical computing, spatial light rebroadcasters (SLRs) require other collaborative devices that provide gain, frequency conversion, and conversion from incoherent to coherent light. Currently, these other devices limit the speed and resolution rather than the SLR.

One possibility is to use the SLR as a spatial light modulator (SLM) for IR rather than as an SLR, as discussed in section 3. Unfortunately, as shown, the CaS samples allow modulation but remove most of the coherency of the passing IR, while the more transparent SrS allows the IR to retain coherency but show negligible modulation. It is possible that the manufacturer could construct a single device that would be useful as an SLM by varying the composition of materials, thickness, and substrate. However, the number of loops through the material is still limited because of power and coherency loss.

The benefits of making an inexpensive thin film modulator with the high resolution and speed of the stimulable electron trapping material is that holograms could be stored and erased in nanosecond time frames without expensive optics. Such fast dynamically variable holograms are not currently possible. This device would be competitive as a storage medium despite the inefficient use of energy. Optical read-write disks are being explored by Optonex. A further illustration is to use the electron trapping material as a coating for other devices which is beyond the scope of the present study.

6.1.1 Optical architectures

There are many experiments that can be performed by using the SLR with other devices in a similar manner to those described. A Hughes LCLV has been ordered that permits IR to be used in reading the LCLV. By using the two LCLVs, one for blue

and the other for IR, it will be possible to construct loops in which many operations may be demonstrated, including experiments with optical learning. The performance and cost are set by these other devices. Unfortunately, the complexity of the systems is limited by having only one such module. The cost of additional devices makes it prohibitive to construct a complicated system. The SLR provides the role of long term memory and permits synchronization. It aids debugging because the machine may be stopped at any point, the status of registers examined, and then the operation continued.

An alternative approach is to design a VLSI chip and mount a ferroelectric liquid crystal light valve on it. Ohio has an NSF Center for Liquid Crystal technology that has offered to work with us on such a project, and we normally make VLSI chips through MOSIS in our VLSI classes and research. In this event, we would experiment with smart pixels. If a sufficiently low cost device is constructed, we could assemble more complex systems. These would not work at high speed, but would enable the programming and control concepts to be tested for optical computer architectures.

7 Conclusions

We surveyed progress in optical digital computing [48]. Recently, microlasers were demonstrated [32] for which the power to drive very high bandwidth signals out of chips is less than that required to drive signals out of electronically connected GaAs VLSI chips. For electronically connected chips, the number of pins is limited and the bandwidth is less than for an optical laser. As a consequence, it is becoming increasingly likely that electronics will move to optically interconnected GaAs VLSI chips which in turn will lead to optical computer architectures. Such optically connected VLSI chips will still need to interact with other devices including memory devices made of different materials such as spatial light rebroadcasters (SLRs).

We performed detailed experiments to characterize SLRs composed of thin films of electron trapping materials on several substrates. The devices have high resolution and speed. Disadvantages for use in digital optical computing are the high attenuation of signal, and an incoherent output of different wavelength to the inputs. Therefore, devices are not cascadable and other devices are needed to restore coherence, restore power level, and convert wavelength. The system performance is now limited by these other devices. Attempts to use the device as a spatial light modulator for IR showed some possibilities

We constructed three modules that have widespread use in digital optical computing. The first was a basic cascadable module using an SLR for long term storage, an image intensifier, and a liquid crystal light valve. The other modules were a binary matrix-vector multiplier and a binary correlator. We showed, using laboratory experiments and simulations, how these modules could be used for performing par-

allel logic, parallel half adders, parallel ripple-carry adders, orthogonal memory, key word addressable holographic memory, interconnections, and optical learning. In fact, many of the subsystems for constructing an optical or hybrid optical digital computer were demonstrated. However, the overall performance was limited in speed and resolution. The cost of the off the shelf devices, needed to work with the SLRs, is such that a complete computer would be prohibitively expensive. The SLR is best suited to long term memory applications where the application depends strongly on their best features.

Future possibilities for making the SLRs more useful include coating the material directly onto other devices and further development of the material into a bistable spatial light modulator. The experience with constructing different subsystems for digital optical computing provided valuable insight into what device characteristics are needed and the difficulties of constructing digital optical computers. In addition to major efforts in all forms of electrooptic device technologies, we recommend the construction of low cost devices for system experiments, even if their performance will not make such systems immediately competitive with electronic computers. This will allow computer engineers and computers scientists to experiment with computer architectures, compiler technologies, and algorithms. The results of such research will suggest new profitable directions for device technology.

References

1. Y. S. Abu-Mostafa and D. Psaltis, "Optical neural computers," Scientific American, **256** (3), p 88-94, 1987.
2. G. P. Agrawal, *Nonlinear fiber optics*, Academic Press, 1989.
3. R. A. Athale and J. N. Lee, "Optical Processing using Outer-Product Concepts," Proc. IEEE **72**, 931-941 (1984).
4. N. F. Borelli, R. H. Bellman, J. A. Durbin, and W. Lama, "Imaging and radiometric properties of microlens arrays," Applied Optics, **30**, 25, pp 3633-3642, 1991
5. K. Brenner, A. Huang, and N. Streibl, "Digital Optical Computing with Symbolic Substitution," Appl. Opt. **25**, 3054-3060 (1986).
6. D. Casasent and B. Telfer, "Key and recollection vector effects on heteroassociative memory performance," Appl. Opt. **28**, 272-283 (1989).
7. T. J. Cloonan and A. L. lentine, "Self-routing crossbar packet switch employing free-sapce optics for chip-to-chip interconnections,", Applied Optics, **30**, 26, pp 3721-3733, 1991.
8. T. H. Cormen, C. E. Leierson, and R. L. Rivest, *Introduction to algorithms*, MIT Press, 1990.
9. R. O. Duda and P. E. Hart, *Pattern classification and scene analysis*, John Wiley, 1973.
10. N. Y. Farhat, D. Psaltis, A. Prata, and E. Paek, " Optical implementation of teh Hopfield model," Applied Optics, **24**, p 1469-1475, 1985.
11. M. R. Feldman, S. E. Esener, C. C. Guest, and S. H. Lee, "Comparison between optical and electrical interconnects based on power and speed considerations," Applied Optics, **27** (9), p 1742-1751, 1988.
12. E. E. Frietman, W. V. Nifterick, L. Kekker, and T. J. M. Jongeling, "Parallel optical interconnects: implementation of optoeletronics in multiprocessor architectures," Applied Optics, **29** (8), pp 1161-1177, 1990.
13. S. Fukushima, T. Kurokawa, and H. Suzuki, "Optical implementation of parallel digital adder and subtractor," Appl. Opt. **29**, 2099-2106 (1990)
14. J. Gasiot, and P. Braunlich, "Nanosecond infrared laser stimulation of luminescence in rare-earth doped sulfides," Appl. Phys. Lett. **40**, (1982).
15. T. K. Gaylord and C. C. Guest, "Optical Digital Truth Table Look-up Processing," Opt. Eng. **24**, 48-58 (1985).
16. J. W. Goodman, A.R. Dias and L. M. Woody, " Fully Parallel, high-Speed Incoherent Optical Method for Performing Discrete Fourier Transforms," Opt. letters, **2**, 1-3 (1977).

17. J. W. Goodman, F. J. Leonberger, S. Y. Kung, and R. A. Athale, "Optical Interconnections for VLSI Systems," Proceedings, IEEE, **72**, pp 85-866, 1984.

18. J. W. Goodman, *Introduction to Fourier Optics*, McGraw-Hill, New York, 1968.

19. M. Govindarajan, "Optically powered arrays for optoelectronic interconnection networks," Applied Optics, p 1335-1346, 1991.

20. K. Hamanaka, "Optical bus interconnectin system using selfoc lenses," Optics Letters, p 1222-1224, 1991.

21. D.O. Hebb, *The Organization of behavior*, (Wiley, New York, 1949).

22. R. Hecht-Nielson, *Neurocomputing* , Addison-Wesley, 1990, p 174

23. L. Hesselink and S. Redfield, "Photorefractive holographic recording in Strontium Barium Niobate fibers", Optics Letters, **13** (10), 1988.

24. A. Huang, "Parallel algorithms for optical digital computers", Technical Digest, IEEE Tenth international Optical Computing Conference, pp 13, 1983.

25. R. G. Hunsperger, *Integrated optics: theory and technology*, Springer Verlag, 1984

26. Hutcheson, L. D. and Haugen, P., "Optical interconnects replace hardwire," IEEE Spectrum, pp 30-35, 1987.

27. K. Hwang and F. A. Briggs, *Computer architecture and parallel processing*, (McGraw-Hill Book Company, New York, 1984).

28. Iga, K, "Microoptics,". In J. W. Goodman, editor, *Inernational trends in optics*, pages 37-55, New York, 1991.

29. M. N. Islam, "Low energy ultrafast fiber soliton logic gates," Opt. Letters, **15**, pp 909-911, 1990.

30. Y. Ichioka, and J. Tanida, "Optical Parallel Logic Gates Using a Shadow-Casting System for Optical Digital Computing", Proc. IEEE **72**, 787-801 (1984).

31. F. Itoh, K. Kitayama, and Y. Tamura, "Learning in optical neural network using erasable optically stimulable phosphor," Optics Letters, 1990.

32. J. L. Jewel, J. P. Harbison, A. and Schere, "Microlasers", Scientific American, **265** (5), 1991.

33. S. Jutamalia, G. M. Storti, J. Lindmeyer, W. Seiderman, "Use of electron trapping materials in optical signal processing 3: Modifiable Hopfield type neural network," Appl. Opt. **30**, 1786-1790 (1990).

34. S. Jutamalia, G. M. Storti, J. Lindmeyer, W. Seiderman, "Use of electron trapping materials in optical signal processing 1: Parallel Boolean Logic," Appl. Opt. **29**, 4806-4811 (1990).

35. J. M. Kinser, H. J. Caulfield, and J. Shamir, "Design for a Massive All-Optical Bidirectional Associative Memory: the Big BAM," Appl. Opt. **27**, 3442-3444 (1988).

36. T. Kohonen, *Self-Organization and Associative Memory*, (Springer-Verlag, New York, 1984).

37. B. Kosko , "Adaptive bidirectional associative memories", Appl. Optics, **26** (23), p 4947-4960, 1987.

38. H. Kogelnik, "Integrated optics, OEICs, or PICs?,". In J. W. Goodman, editor, *Inernational trends in optics*, pages 1-12, New York, 1991.

39. R. K. Kostuk, J. W. Goodman, and L. Hesselink, "Optical imaging applied to microelectronic chip-to-chip interconnections," Applied Optics, **24**, pp 2851-2858, 1985

40. E. N. Leith and J. Uptaneieks, "Reconstructed wavefronts and communication theory", J. Optical Soc. America, **52**, pp 1123, 1962.

41. E. N. Leith and J. Uptaneieks, "Wavefront reconstruction eith diffused illumination and three-dimensional objects", J. Optical Soc. America, **54**, pp 1295, 1964.

42. Lin, F., Strzelecki, E. M., and Jannson, T., "Optical multiplanar VLSI interconnect based on multiplexed waveguide holograms," Applied Optics, **29**, pp 1126-1133, 1990.

43. H. Liu, S. Y. Kung, and J. A. Davis, "Real-Time Optical Associative Retrieval Techniques," Optical Engineering, **25**, 853-856, 1986.

44. S. H. Lee, "Nonlinear optical processing," in, *Optical Information Processing*, Ed. S. H. Lee, (Springer-Verlag, New York, 1981).

45. S. G. Mallat, "A Theory for Multiresolution Signal Decomposition: The Wavelet Transform," IEEE Trans. Pattern Analysis and Machine Intelligence, July 1989.

46. A. D. McAulay, J. Wang, X. Xu, M. Zeng, "Optical parallel set of full adders using spatial light rebroadcasters", SPIE Optical Information and Processing Systems and Architectures II Conference, **1564**-64, July 1991.

47. A. D. McAulay, J. Wang, and X. Xu, "Optical adder using spatial light rebroadcasters", Submitted to Applied Optics, 1991.

48. A. D. McAulay, *Optical computer architectures*, (John Wiley, New York, 1991).

49. A. D. McAulay, "Optical implementation of a novel accurate-location radar and sonar", Optical Engineering, **30** (10), p 1511-1515, 1991.

50. A. D. McAulay, J. Wang, X. Xu, and M. Zeng, "Demonstration of optical learning with luminescent materials for image classification," IEEE Intl. Conf. on Systems, Man, and Cybernetics, Oct. 1991.

51. A. D. McAulay, J. Wang, and C. T. Ma, "Optical heteroassociative memory using spatial light rebroadcasters (SLRs)," Appl. Opt. **29**, 2067-2073 (1990).

52. A. D. McAulay, "Logic and Arithmetic with Luminescent Rebroadcasting Devices," Proc. Soc. Photo-Opt. Instrum. Eng. **936**, 321-326 (1988).

53. A. D. McAulay and J. Wang, "Spatial light rebroadcaster bit-slice word-addressable holographic memory," Appl. Opt. **30**, p 2885-2889, 1991.

54. A. D. McAulay, J. Wang, and C. T. Ma, "Optical Dynamic Matched Filtering with Electron Trapping Devices," Proc. Soc. Photo-Opt. Instrum. Eng. **977**, 271-276 (1988).

55. A.D. McAulay, "Real-time optical expert systems", Applied Optics, **26**(10), p 1927-1934, 1987.

56. F. B. McCormick, "Optical circuitry for free space interconnections," Applied Optics, **29** p 2013-2018, 1991.

57. D. A. B. Miller, "Quantum wells for optical information processing," Optical Engineering, **26**, (5), pp 386-372, 1987

58. M. J. Murdocca, A. Huang, J. Jahns, and N. Streibl, " Optical design of programmable logic arrays," Appl. Opt. **27**, 1651-1660 (1988).

59. M. J. Murdocca, "Digital optical computing with one-rule cellular automata," Applied Optics, **26**, pp 682-688, 1987

60. J. A. Neff, R. A. Athale, and S. H. Lee, "Two-Dimensional Spatial Light Modulators: A Tutorial," Proceedings, IEEE, **78**, 826-855, 1990.

61. A. V. Oppenheim and R. W. Schafer, *Digital Signal Processing*, Prentice-Hall, 1975.

62. Y. Owechko, G. J. Dunning, E. Marom, and B. H. Soffer, "Holographic associative memory with nonlinearities in the correlation domain,," Appl. Opt. **26**, 1900-1910 (1987).

63. R. Paturi, "Parallel algorithms based on expander graphs for optical computing,;,, Applied Optics, , p 917-927, 1991.

64. D. Psaltis, D. Brady, and K. Wagner, "Adaptive optical networks using photorefractive crystals," Applied Optics, **27**, 1752-1759, 1988.

65. N. A. Riza, and D. Psaltis, "Acousto-optic signal processors for transmission and reception of phased-array antenna signals," Applied Optics, **30**, 23, pp 3294-3303, 1991

66. F. Rosenblatt, *Principles of neurodynamics: Perceptrons and the theory of brain mechanism*, Spartan, Washington, 1961.

67. D. E. Rumelhart, G. E. Hinton, and R. J. Williams, "Learning Internal Representations by Error Propagation", in Rumelhart, D. E. and McCleiland, J. L., eds., *Parallel Distributed Processing: Explorations in the Microstructure of Cognition, Vol-1 : Foundations,* MIT Press, 1986.

68. A. Ayyalusamy, "Cellular automata-based multiplier for optical computers", Master's thesis, Wright State University, 1991.

69. I. Satoh, M. Kato, K. Fujito, and F. Tateishi, "Holographic memory system for Kanji character generation", Applied Optics, **28**, (13), pp. 2634-2640, 1989.

70. T. Shiono, and H. Ogawa, "Diffraction-limited blazed reflection diffractive microlenses for oblique incidence fabricated by electron-beam lithography," Applied Optics, **30**, 25, pp 3643-3649, 1991

71. D. Sun and Z. Weng, "Butterfly interconnection implementation for an n-bit parallel ripple carry full adder," Appl. Opt. **30**, 1781-1785 (1991).

72. G. W. Taylor, J. G. Simmons, A. Y. Cho, and R. S. Mand, "A New Double Heterostructure Optoelectronic Switching Device Using Molecular Beam Epitaxy," Applied Physics, **59**, p 596-600, 1986.

73. B. Telfer and D. Casasent, "Updating optical pseudoinverse associative memories," Appl. Opt. **28**, 2518-2528 (1989).

74. J. Tanida, J. Nakagawa, E. Yagyu, M. Fukui, and Y. Ichioka, "Experimental verification of parallel processing on a hybrid parallel array logic system," Appl. Opt. **29**, 2510-2521 (1990).

75. A. B. Vander Lugt, "Signal Detection by Complex Spatial Filtering", IEEE Trans. Info. Theory, **IT-10**, (2), 1964

76. T. Y. Young and T. W. Calvert, *Classification, estimation and pattern recognition*, Elsevier, 1974.